Anti-diffusive alternate-directions schemes for the transport of step functions

Léa Batteux, Fabien Duval, Raphaele Herbin, Jean-Claude Latché, Pascal Poullet

ANTI-DIFFUSIVE ALTERNATE-DIRECTIONS SCHEMES FOR THE TRANSPORT OF STEP FUNCTIONS

L. Batteux[1], F. Duval[2], R. Herbin[3], J.-C. Latché[4] and P. Poullet[5]

Abstract. The purpose in this paper is to design finite-volumes schemes on structured grids for the transport of piecewise-constant functions (typically, indicator functions) with as low diffusion as possible. We first propose an extension of the so-called Lagrange-projection algorithm, or downwind scheme with an Ultrabee limiter, for the transport equation in one space dimension with a non-constant velocity; as its constant velocity counterpart, this scheme is designed to capture the discontinuities separating two plateaus in only one cell, and is referred to as "anti-diffusive". It is shown to preserve the bounds of the solution. Then, for two and three dimensional problems, we introduce a conservative alternate-directions algorithm, an show that this latter enjoys a discrete maximum principle, provided that the underlying one-dimensional schemes satisfy a property which may be seen as a flux limitation, possibly incorporated *a posteriori* in any explicit scheme. Numerical tests of this alternate-directions algorithm are performed, with a variety of one-dimensional embedded schemes including the anti-diffusive scheme developed here and the so called THINC scheme. The observed numerical diffusion is indeed very low. With the anti-diffusive scheme, the above-mentionned *a posteriori* limitation is necessary to preserve the solution bounds, but, in the performed tests, does not introduce any visible additional diffusion.

2010 AMS Subject Classification. — Please, give AMS classification codes —.

The dates will be set by the publisher.

1. Introduction

We address in this paper the following problem, posed over a domain Ω of $\mathbb{R}^d$, $d = 1,\ 2,\ 3$,

$$\partial_t y + \mathrm{div}(y\,\boldsymbol{u}) = 0, \quad \mathrm{div}(\boldsymbol{u}) = 0, \tag{1}$$

where y is a scalar variable, *i.e.* a function from Ω to $\mathbb{R}$ and $\boldsymbol{u}$ stands for a velocity field. We pay a special attention to the cases where y is a step function, such as the indicator function in multiphase flow problems like liquid-solid flows or liquid-gas flows dealt with by the so-called Volume-Of-Fluid (VOF) method.

The aim of this paper is to study some recent finite-volume schemes to solve (1) which have been designed to reduce the numerical diffusion as much as possible and to propose some (to ourknowledge) novel variants. More precisely speaking, we first introduce some schemes for the one-dimensional transport with a non-constant velocity:

- We first propose an extension to the non-constant velocity case of the Lagrange-projection introduced in [5] for constant velocity flows. The original scheme enjoys the property of exactly transporting the Heaviside function (and so, in fact, any step function, see [5]), and the proposed extension is designed to satisfy a similar property, namely the fact that a discontinuity is captured in only one cell. We show in addition that it satisfies a local discrete maximum principle.
- Then we recall a class of schemes based on a reconstruction-transport-projection paradigm, focusing on the so called THINC scheme where the reconstruction is performed by a hyperbolic tangent profile [4]. We show that this scheme also satisfies a local discrete maximum principle.

Keywords and phrases: Finite-volume schemes, transport, antidiffusion, maximum principle.

[1] Université des Antilles (lea.batteux@univ-antilles.fr)

[2] IRSN, BP 13115, St-Paul-lez-Durance Cedex, France (fabien.duval@irsn.fr)

[3] I2M UMR 7373, Aix-Marseille Université, CNRS, Ecole Centrale de Marseille. 39 rue Joliot Curie. 13453 Marseille, France (raphaele.herbin@univ-amu.fr)

[4] IRSN, BP 13115, St-Paul-lez-Durance Cedex, France (jean-claude.latche@irsn.fr)

[5] Université des Antilles (pascal.poullet@univ-antilles.fr)

- Finally, for comparison purposes, we include in the study a standard MUSCL-like scheme based on an algebraic limitation of the reconstructed interface values [13].

Then we turn to the implementation of these schemes to multi-dimensional problems on structured meshes thanks to the alternate-direction technique. As already stated in [2, Section 3.1], preserving the maximum principle at each step may force to give up conservativity. Let us explain this issue in the time-semi-discrete setting, for instance for a two-dimensional problem. Let y^n, $y^{(1)}$ and y^{n+1} be the approximation of y at time t_n, after a step of transport in the first direction and at t_{n+1} respectively, and let us denote by $\boldsymbol{u}^{(1)}$ (resp. $\boldsymbol{u}^{(2)}$) the vector function defined by $\boldsymbol{u}^{(1)} = (u^{(1)}, 0)^t$ (resp. $\boldsymbol{u}^{(2)} = (0, u^{(2)})^t$), where $u^{(1)}$ (resp. $u^{(2)}$) is the first (resp. second) component of the velocity field $\boldsymbol{u}$. In the general case, $\boldsymbol{u}^{(1)}$ and $\boldsymbol{u}^{(2)}$ are not divergence-free. The time discretization is performed with a forward Euler time; the alternate-direction algorithm, switching to a transport formulation of Equation (1) to preserve the maximum principle thus reads:

$$\text{Transport in the first direction} \qquad \frac{1}{\delta t}\left(y^x - y^n\right) + \operatorname{div}(y^n \boldsymbol{u}^x) - y^n \operatorname{div}(\boldsymbol{u}^x) = 0,$$

$$\text{Transport in the second direction} \qquad \frac{1}{\delta t}\left(y^{n+1} - y^x\right) + \operatorname{div}(y^x \boldsymbol{u}^y) - y^x \operatorname{div}(\boldsymbol{u}^y) = 0,$$

with δt the time-step. Observe that the non-conservativity stems from the difference in the factor multiplying $\operatorname{div}(\boldsymbol{u}^{(1)})$ and $\operatorname{div}(\boldsymbol{u}^{(2)})$ in the first and second equation, respectively. A conservative algorithm may thus be recovered, for instance, by switching from $y^{(1)} \operatorname{div}(\boldsymbol{u}^{(2)})$ to $y^n \operatorname{div}(\boldsymbol{u}^{(2)})$ in the second equation, but the price to pay seems to be to loose the maximum principle. Surprisingly, this is not so. In fact, we show that the maximum principle is satisfied when the one-dimensional scheme is the above mentioned MUSCL scheme; moreover, it also satisfied for the antidiffusive schemes introduced in Section 2 provided that they satisfy an additional limitation. The resulting algorithms are compared on classical benchmarks for volume of fluid (VOF) schemes.

Another extension to non-constant velocity flows of the Lagrange-projection scheme, in one space dimension, may be found in [1]. It notably differs from the present formulation; indeed, the velocity is supposed to be given at the cell centers in this latter work, while it is supposed to be known at the faces of the mesh in the present work, in view of an implementation of the proposed transport scheme in a staggered discretization of hydrodynamics (typically, to transport a phase indicator function in a flow computed by the so-called Marker-And-Cell (MAC) scheme [8, 9]).

The paper is organized as follows. The considered schemes for the one-dimensional transport are introduced in Section 2. Their implementation in an alternate-directions algorithm is discussed in Section 3 and Section 4 is devoted to numerical tests.

2. Schemes for one-dimensional transport

We gather in this section the presentation of the one-dimensional schemes which are used as elementary building bricks for the alternate-direction algorithms tested in Section 4. In Section 2.1, for the convenience of the reader, we first recall with our notations the scheme and the related results presented in [5], in the specific case of the one-dimensional transport by a constant velocity field. Precisely speaking, we recast this scheme as a downwind scheme, whose positivity is preserved by a CFL-dependent limiter; such a construction may also be found in [15] (where the scheme is referred to as the Ultrabee scheme) and is recalled in [11] (where the limiter is referred to as the upper-bound limiter). We propose an extension of this scheme to the variable velocity transport problem in Section 2.2; in this same section, we show that, under a CFL condition, this extension satisfies a local maximum principle. In Section 2.3, we recall some schemes already introduced in the literature [4], which, as the Lagrange-projection scheme, consist in performing a reconstruction of the unknown, and then compute the flux through a face by a Godunov technique; we prove for this schemes a local maximum principle. Finally, we briefly recall in section 2.4 a MUSCL scheme (see *e.g.* [7, 11] for the general formalism and [13] for the same presentation as here), which is implemented for comparison purposes. The numerical results are shown in Section 4.

2.1. **The Lagrange-projection algorithm for the 1D constant velocity case**

We deal here with the following model problem:

$$\partial_t y + u\ \partial_x y = 0, \qquad u \in \mathbb{R},\ u \geq 0.$$

Let y_-, y and y_+ be the value taken by the unknown in three successive cells, sorted from left to right. We denote by K the middle cell and by σ the interface between K and the right cell (see Figure 1). The numerical flux through σ outward K reads $G_{K,\sigma} = u\, y_\sigma$ and our aim is to give a value for the approximation at the face y_σ. We begin with the case where K does not correspond to a (local) maximum (*i.e.* we suppose $(y - y_-)\,(y_+ - y) \geq 0$ and either $y \neq y_-$ or $y \neq y_+$) and, without loss of generality, we assume $y_- \geq y$ and $y \geq y_+$, with $y_- > y_+$.

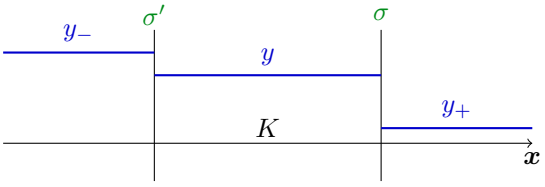

FIGURE 1. Notations for the one-dimensional problem

The Lagrange-projection algorithm involves two steps: first, a reconstruction of the unknown in the cell K supposing that the unknown is a step function taking the value y_- on the left part of K and the value y_+ on the right part, y being the average of the unknown over K (see Figure 2); second, the computation of $G_{K,\sigma}$ as the integration over the time-step of the actual flux of the reconstructed function.

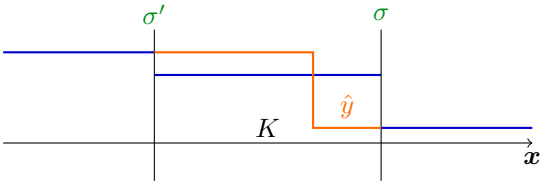

FIGURE 2. Reconstruction step – Blue: initial function. Red: reconstructed function in cell K

To alleviate the notations, we suppose that $K = (0, \delta x)$ and that the time interval under consideration is $(0, \delta t)$ The reconstructed function $\hat{y}$ over K, at the beginning of the time step so at $t = 0$, reads:

$$\hat{y}(x,0) = y_- \text{ if } x \leq \xi\,\delta x,\ \hat{y}(x,0) = y_+ \text{ otherwise, with } \xi = \frac{y_+ - y}{y_+ - y_-}. \tag{2}$$

Let ν be a CFL number, defined by $\nu = \frac{u\,\delta t}{\delta x}$. For $t \leq \frac{\delta x}{u}$, the transport of $\hat{y}$ at the velocity u yields

$$\hat{y}(\delta x, t) = \begin{cases} y_+ & \text{if } t \leq \dfrac{(1-\xi)\,\delta x}{u}, \\ y_- & \text{otherwise.} \end{cases}$$

Integrating over $(0, \delta t)$, we obtain that the numerical flux $G_{K,\sigma}$ through σ outward K satisfies:

$$\delta t\ G_{K,\sigma} = \begin{cases} \delta t\ u\, y_+ & \text{if } \delta t \leq \dfrac{(1-\xi)\,\delta x}{u}, \\ (1-\xi)\,\delta x\, y_+ + (u\,\delta t - (1-\xi)\,\delta x)\, y_- & \text{otherwise.} \end{cases}$$

Since, by definition of y_σ, we have $G_{K,\sigma} = u\ y_\sigma$, we get

$$y_\sigma = \begin{cases} y_+ & \text{if } \nu \leq 1-\xi, \\ \bar{y}_\sigma \coloneqq \dfrac{1-\xi}{\nu}\ y_+ + (1 - \dfrac{1-\xi}{\nu})\ y_- & \text{otherwise.} \end{cases}$$

Using (2), we get:

$$\bar{y}_\sigma = y_- - \frac{1}{\nu}\ (y_- - y). \tag{3}$$

Seen as a function of ν, for $\nu \in (0,1]$, $\bar{y}_\sigma$ increases, from $-\infty$ (ν tending to zero) to y for $\nu = 1$. In addition, thanks to (2), $\nu = 1-\xi$ implies $\bar{y}_\sigma = y_+$. The behaviour of $\bar{y}_\sigma(\nu)$ as a function of ν thus shows the equivalence between the two conditions $\nu \leq (1-\xi)$ and $\bar{y}_\sigma(\nu) \leq y_+$, and the expression of y_σ may be recast as $y_\sigma = y_+$ if $\bar{y}_\sigma \leq y_+$ and $\bar{y}_\sigma$ otherwise, or just simply $y_\sigma = \max(y_+, \bar{y}_\sigma)$, so that y_σ can be chosen as the projection of y_+ on the interval $[\bar{y}_\sigma, +\infty[$.

Moreover, in the case where y is a local maximum (*i.e.* $(y - y_-)\,(y_+ - y) < 0$ or $y_- = y = y_+$), the definition of the reconstructed function $\hat{y}$ is not possible; the upwind choice $y_\sigma = y$ seems reasonable, and it is in fact the only one which ensures a discrete maximum principle, as we will see later. For this latter reason, the value y_σ is finally chosen as the projection of y_+ on the interval $[\bar{y}_\sigma, y]$ and is obtained by the following two-step computation:

(i) choose y_+ as tentative value for y_σ,

(ii) define

$$I_\sigma = [\ y - \frac{1-\nu}{\nu}\ (y_- - y), y]$$

as admissible interval and project the tentative value y_+ over I_σ.

It is straightforward to check that the same conclusion may be drawn in the case where the unknown is increasing (*i.e.* $y_- \leq y \leq y_+$ with $y_- < y_+$). We have thus recast, in the present specific case, the Lagrange-projection algorithm as a downwind scheme with a suitable limitation, corresponding to the case where the reconstructed front is beyond the edge σ. This scheme is known to preserve the discrete maximum principle, and to transport the Heaviside function exactly (and therefore, by an easy extension, any step function) in the following sense: at each time, the discrete solution in a cell corresponds to the mean value of the exact solution [5].

2.2. **An algorithm preserving the step functions for the 1D transport**

Let us then consider the problem

$$\partial_t y + u(x,t)\ \partial_x y = 0, \tag{4}$$

where the velocity u is now possibly variable in space and time. The objective of this section is to derive a scheme that will both preserve the maximum principle and transport the step functions exactly, following the ideas of Section 2.1.

The scheme. - For the solution of Equation (4), a derivation of the scheme based on the (exact) transport of a reconstructed function for the unknown y is not straightforward, since the velocity is not constant and thus the transport would necessitate a reconstruction of the velocity itself. Since we showed in the previous section that, in the constant velocity case,the recontruction leads to downwind limited scheme, we propose to follow this idea: we thus write a finite volume scheme as a downwind limited scheme as in Section 2.1, and then tunethe limitation in order to obtain a non-diffusive approximation of step functions, in the sense that the transition from one plateau to the another one is captured in only one cell.

The discrete form of the transport equation satisfied by y is obtained by a discretization of the equation $\partial_t y + \partial_x(u\,y) - \partial_x(u)\ y = 0$, with a finite volume approximation of the divergence operators. Using the notations of Section 2.1 and denoting by u_σ and $u_{\sigma'}$ an approximation of the velocity over the time interval $[t_n, t_{n+1}]$ and at the faces σ and σ' respectively, this equation reads for the cell K:

$$\frac{|K|}{\delta t}\ (y^{n+1} - y) + u_\sigma\,(y_\sigma - y) - u_{\sigma'}\,(y_{\sigma'} - y) = 0,$$

or, equivalently:

$$y^{n+1} = y - \text{sign}(u_\sigma)\ \nu\ (y_\sigma - y) + \text{sign}(u_{\sigma'})\ \nu'\ (y_{\sigma'} - y), \tag{5}$$

with

$$\nu = \frac{\delta t\ |u_\sigma|}{|K|}, \quad \nu' = \frac{\delta t\ |u_{\sigma'}|}{|K|}. \tag{6}$$

To design the limitation process, we consider a specific case. We suppose that $u_\sigma \geq 0$, $u_{\sigma'} \geq 0$ and, in all the cells at the left (resp. right) side of K, the unknown is equal to $y_- > 0$ (resp. is equal to 0), with $y_- \geq y \geq 0$ (note that the left-hand side of Equation (5) vanishes when the unknown is constant, so the present construction trivially extends to $y_+ \neq 0$); in this case, we expect the scheme to allow y^{n+1} to take the value y_- (just) before limitation, as occurs in the constant velocity case. In addition, we suppose that the scheme imposes $y_{\sigma'} = y_-$ (and we will check *a posteriori* that it is indeed the case) and that it is a downwind limited scheme, *i.e.* that $y_\sigma = 0$ if the limitation is not active. Equation (5) yields:

$$y^{n+1} = y - \nu\ (y_\sigma - y) + \nu'\ (y_- - y),$$

so that we have, at the point where limitation becomes active,

$$y_- = y - \nu\ (\bar{y}_\sigma - y) + \nu'\ (y_- - y),$$

i.e.

$$\bar{y}_\sigma = y + \frac{1 - \nu'}{\nu}\ (y - y_-).$$

By the same arguments as in the previous section (monotonicity of $\bar{y}_\sigma$ with respect to the time step, and $\bar{y}_\sigma$ tends to $-\infty$ when the time step tends to zero), this result suggest that y_σ may be obtained by the projection of $y_+ = 0$ over the interval

$$I_\sigma = [y - \frac{1 - \nu'}{\nu}\ (y_- - y), y].$$

This computation suggests the following choice for the values y_σ and y'_σ in the finite volume scheme (5):

$$\text{for } \tau \in \mathcal{E},\ y_\tau \text{ is the projection of the downwind value } y_{\text{dw}} \text{ onto } I_\tau = \Big[\ y_{\text{uw}} - \frac{1 - \nu_{\text{op}}}{\nu_\tau}\ (y_{\text{op}} - y_{\text{uw}}), y_{\text{uw}}\Big], \tag{7}$$

where y_{uw} is the value in the cell K_{uw} upwind to τ, ν_τ (resp.ν_{op}) is the CFL number defined by Equation (6) associated to the face τ (resp. to the face σ_{op} opposite to τ in K_{uw}) and y_{op} is the value of the unknown in the cell separated from K_{uw} by σ_{op} (see Figure 3). Since y_σ is obtained by projection of y_{dw} onto an interval containing y_{uw}, we observe that y_τ is a convex combination of y_{dw} and y_{uw}. Note also that, when $(y_{\text{op}} - y_{\text{uw}})\ (y_{\text{uw}} - y_{\text{dw}}) \leq 0$ (*i.e.* when y_{uw} is a local extremum), the projection of y_{dw} onto I_τ is y_{uw} (so, as usual in this case, the scheme boils down to the upwind scheme). Returning to the example used to build the scheme, since the unknown is supposed to be equal to y_- in the (at least two) cells located on the left side of σ', the computation (7) for σ' yields $I_{\sigma'} = \Big[\ y_{\text{uw}}, y_{\text{uw}}\Big]$, so that $y_{\sigma'} = y_{\text{uw}} = y_-$, which we assumed the scheme would yield, and which is thus confirmed *a posteriori*; by construction, the scheme thus captures such a discontinuity in only one cell.

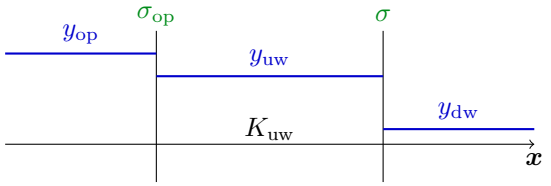

FIGURE 3. Computation of y_σ for the configuration above ($u_\sigma \geq 0$, $u_{\sigma'} \geq 0$).

Checking the discrete maximum principle. - We begin with the following elementary lemma.

Lemma 2.1. *Let a, b and c be three real numbers, with $a \leq b \leq c$. Let*

$$m = (1 - \alpha - \beta)\, b + \alpha a + \beta c,$$

with $0 \leq \alpha \leq 1$ and $0 \leq \beta \leq 1$. Then $m \in [a, c]$.

Proof. Note that m is not a convex combination of a, b and c, since $1-\alpha-\beta$ may become negative. However,

$$m = \begin{cases} (1-\beta)\, a + \beta c, \text{ if } b = a \\ (1-\alpha)\, c + \alpha a, \text{ if } b = c, \end{cases}$$

so that in both cases, m is a convex combination of a and c. Since $b \in [a, c]$ and since m depends linearly on b, it follows that $m \in [a, c]$ for any $b \in [a, c]$. □

Remark 2.2 (Lemma 2.1 and TVD criterium)**.** The purpose of this lemma is to be applied with $m = y^{n+1}$, $b = y$ and either $a = y_-$ and $c = y_+$ or $a = y_+$ and $c = y_-$. Once this substitution done, it may look as the usual criterium which implies that the scheme is TVD [10], namely the fact that y^{n+1} is a convex combination of y_-, y and y_+. However, the range of variation of the coefficients α and β is here larger (and this is crucial for the scheme under consideration), since their sum is only required to be lower than 2, and the coefficient of b (or y) may consequently be negative.

We now check that the scheme (7) satisfies a local maximum principle, in the following sense.

Lemma 2.1 (Discrete local maximum principle)**.** *With the notations of the beginning of the section, let us suppose that the face CFL numbers ν and ν' defined by Equation* (6) *are such that $\nu \leq 1$ and $\nu' \leq 1$; let us suppose in addition that, if $u_\sigma \leq 0$ and $u_{\sigma'} \geq 0$ (*i.e. *the flow is entering the cell K through its two faces), $\nu + \nu' \leq 1$. Then*

$$y^{n+1} \in [\min(y_-, y, y_+), \max(y_-, y, y_+)].$$

Proof. Let us first suppose that y is not a local extremum, and let us consider all the possible configurations according to the sign of u_σ and $u_{\sigma'}$:

- **Case 1:** $u_\sigma \geq 0$ and $u_{\sigma'} \geq 0$ – The scheme reads

$$y^{n+1} = y - \nu\,(y_\sigma - y) + \nu'\,(y_{\sigma'} - y)$$

By (7), there exists $\alpha \in [0, 1]$ such that $y_\sigma - y = \alpha\, \dfrac{1-\nu'}{\nu}\, (y - y_-)$. Moreover, recall that, owing to (7), $y_{\sigma'}$ is a convex combination of y_- and y; therefore there exists $\alpha' \in [0, 1]$ such that

$$y_{\sigma'} - y = \alpha'\,(y_- - y).$$

we thus get

$$y^{n+1} = \Big(1 - \big((1-\nu')\,\alpha + \nu'\,\alpha'\big)\Big)\; y + \big((1-\nu')\,\alpha + \nu'\,\alpha'\big)\; y_-.$$

The quantity $(1-\nu')\,\alpha + \nu'\,\alpha'\big)$ is a convex combination of α and α' and thus lies in the interval $[0, 1]$; y^{n+1} is thus a convex combination of y and y_-.

- **Case 2:** $u_\sigma \leq 0$ and $u_{\sigma'} \leq 0$ – Similar arguments yield that y^{n+1} is a convex combination of y and y_+.
- **Case 3:** $u_\sigma \leq 0$ and $u_{\sigma'} \geq 0$ – The scheme reads

$$y^{n+1} = y + \nu\,(y_\sigma - y) + \nu'\,(y_{\sigma'} - y)$$

and, again owing to (7), there exists $\alpha \in [0, 1]$ and $\alpha' \in [0, 1]$ such that

$$y_\sigma - y = \alpha\,(y_+ - y), \qquad y'_\sigma - y = \alpha'\,(y_- - y).$$

We thus get

$$y^{n+1} = \left(1 - \alpha\,\nu - \alpha'\,\nu'\right)\, y + \alpha\,\nu\, y_+ + \alpha'\,\nu'\, y_-$$

and, by assumption, we have $\nu + \nu' \leq 1$, so y^{n+1} is a convex combination of y_-, y and y_+.

- **Case 4:** $u_\sigma \geq 0$ and $u_{\sigma'} \leq 0$ – The scheme reads

$$y^{n+1} = y - \nu\,(y_\sigma - y) - \nu'\,(y_{\sigma'} - y)$$

and there exists $\alpha \in [0,1]$ and $\alpha' \in [0,1]$ such that

$$y_\sigma - y = \alpha\,\frac{1-\nu'}{\nu}\,(y - y_-), \qquad y'_\sigma - y = \alpha'\,\frac{1-\nu}{\nu'}\,(y - y_+).$$

We thus get

$$y^{n+1} = \left(1 - \alpha\,(1-\nu') - \alpha'\,(1-\nu)\right)\, y + \alpha\,(1-\nu')\, y_- + \alpha'\,(1-\nu)\, y_+,$$

and, thanks to Lemma 2.1, y^{n+1} is a convex combination of y_- and y_+.

Let us now turn to the case where y is a local extremum. The only difference with the "monotone case" is that Lemma 2.1 no longer applies. However, this lemma is invoked only in Case 4, where the flow leaves K through its two faces, so K is the upwind cell for σ and σ' ; we are thus in the case where the upwind value is an extremum, and $y_\sigma = y_{\sigma'} = y$, which yields $y^{n+1} = y$. □

Remark 2.3 (On the limitation $\nu + \nu' \leq 1$)**.** To deal with Case 3, we could invoke Lemma 2.1, so the limitation $\nu + \nu' \leq 1$ is useful only in the pathological case where the flow enters the cell through its two faces, and the solution has a local extremum in this cell. Unfortunately, this can really happen: for instance, if the solution is 0 except in the considered cell, where its takes the value 1, we have $y^{n+1} = 1 - \nu - \nu'$, and, if $\nu + \nu' > 1$, the solution becomes negative.

2.3. **Reconstruction-based algorithms for the 1D transport**

The Lagrange-projection scheme presented in Section 2.1 is a reconstruction-based algorithm, with a step function for the reconstruction profile. The reconstruction step may be performed with another monotone function than the step function. For instance, the so-called THINC-M scheme presented in [4] performs a reconstruction by a hyperbolic tangent function; the practical computations for this scheme are given, for the sake of completeness, in Section A of the appendix. Let us show that the class of schemes obtained with these various reconstructions still satisfy the maximum principle.

With the same notations as in the previous section, let $\sigma \in \mathcal{E}$, and $K_{\rm uw}$ be the upwind cell. Let us suppose that $K_{\rm uw}$ is not a local extrema, *i.e.* that $(y_{\rm uw} - y_{\rm dw})\,(y_{\rm op} - y_{\rm uw}) > 0$ and let $\tilde{y}$ be a monotone real-valued function satisfying the following assumptions:

$$\lim_{{\rm sgn}(u_\sigma)x \to -\infty} \tilde{y}(x) = y_{\rm op}, \quad \lim_{{\rm sgn}(u_\sigma)x \to +\infty} \tilde{y}(x) = y_{\rm dw}, \quad \int_{K_{\rm uw}} \tilde{y}(x)\ {\rm d}x = |K_{\rm uw}|\ y_{\rm uw}.$$

Then, the flux from $K_{\rm uw}$ through the face σ is evaluated by

$$G_{K_{\rm uw},\sigma} = \frac{1}{\delta t}\ {\rm sgn}(u_\sigma)\ \int_{x_\sigma - u_\sigma\,\delta t}^{x_\sigma} \tilde{y}(x)\ {\rm d}x,$$

where x_σ stands for the coordinate of the face σ. In the other case, *i.e.* if $K_{\rm uw}$ is a local extremum, $G_{K_{\rm uw},\sigma}$ is computed by the standard first-order upwind scheme.

For the sake of simplicity and without loss of generality, assume that $K_{\rm uw} =]0,1[$ and $x_\sigma = 1$, which implies $u_\sigma \geq 0$, since $K_{\rm uw}$ is the upwind cell with respect to σ. Then,

$$G_{K_{\rm uw},\sigma} = \frac{1}{\delta t}\ \int_{1-\nu}^{1} y(x)\ {\rm d}x,$$

so that the edge value y_σ defined by $G_{K_{\rm uw},\sigma} = |u_\sigma|\ y_\sigma$ reads

$$y_\sigma = \frac{1}{\nu}\int_{1-\nu}^{1} \tilde{y}(x)\ \mathrm{d}x. \tag{8}$$

Let us suppose that $K_{\rm uw}$ is not a local extremum and that $y_{\rm op} \le y_{\rm uw} \le y_{\rm dw}$. Then we have:

$$y_\sigma - y_{\rm uw} = \frac{1}{\nu}\int_{1-\nu}^{1} (\tilde{y}(x) - y_{\rm uw})\ \mathrm{d}x;$$

remarking that

$$\int_{K_{\rm uw}} (\tilde{y}(x) - y_{\rm uw})\ \mathrm{d}x = 0,$$

we get

$$y_\sigma - y_{\rm uw} = -\frac{1}{\nu}\int_{0}^{1-\nu} (\tilde{y}(x) - y_{\rm uw})\ \mathrm{d}x.$$

Since $\tilde{y}$ is a monotone function, $\tilde{y}(x) \ge y_{\rm op}$ for $x \in K_{\rm uw}$ and therefore

$$y_\sigma - y_{\rm uw} \le \frac{1-\nu}{\nu}\ (y_{\rm uw} - y_{\rm op}).$$

In addition, since $\tilde{y}$ is a non-decreasing function, its mean value of $(1-\nu, 1)$ with $\nu \le 1$ cannot be lower than its mean value over $(0,1)$, so that, owing to (8), $y_\sigma \ge y_{\rm uw}$; moreover, since $\tilde{y}(x) \le y_{\rm dw}$ for $x \in (0,1)$, we finally get $y \in [y_{\rm uw}, y_{\rm dw}]$. By similar arguments in the case $y_{\rm op} \ge y_{\rm uw} \ge y_{\rm dw}$ and since $y_\sigma = y_{\rm uw}$ if $K_{\rm uw}$ is a local extremum, we obtain that y_σ is a convex combination of $y_{\rm uw}$ and $y_{\rm dw}$ and satisfies

$$y_\sigma \in I_\sigma = [y_{\rm uw},\ y_{\rm uw} + \frac{1-\nu}{\nu}\ (y_{\rm uw} - y_{\rm op})].$$

By the same arguments as in the previous section, if the face CFL numbers are all lower than 1, the scheme satisfies a local maximum principle in the sense that $y_{\rm uw}^{n+1}$ is a convex combination of $y_{\rm op}$, $y_{\rm uw}$ and $y_{\rm dw}$.

2.4. **A MUSCL scheme**

With the notations of Section 2.2, a MUSCL scheme may be obtained by the following choice for the interpolation of the unknown at the face, for $\sigma \in \mathcal{E}$ located at x_σ:

$$\begin{array}{ll} (i) & \text{first, let } \tilde{y}_\sigma \text{ be an affine interpolate between } y_{\rm uw} \text{ and } y_{\rm dw} \text{ at } x_\sigma, \\ (ii) & \text{then obtain } y_\sigma \text{ as the projection of } \tilde{y}_\sigma \text{ onto } I_\sigma \\ & \text{with } I_\sigma = \mathcal{I}(y_{\rm uw} + \ (y_{\rm op} - y_{\rm uw}), y_{\rm uw}), \text{ and, for } a, b \in \mathbb{R}, \mathcal{I}(a,b) = \begin{cases} [a,b] \text{ if } a \le b, \\ [b,a] \text{ otherwise.} \end{cases} \end{array} \tag{9}$$

We recall that $y_{\rm uw}$ and $y_{\rm dw}$ are the value taken by the unknown in the cell upwind to σ and downwind to σ, respectively, and $y_{\rm op}$ is the value of the unknown in the opposite cell to σ with respect to the upwind cell.

As for the anti-diffusive scheme, since y_σ is obtained by projection of a convex combination of $y_{\rm uw}$ and $y_{\rm dw}$ onto an interval containing $y_{\rm uw}$, y_σ is a convex combination of $y_{\rm dw}$ and $y_{\rm uw}$. As usual, also, when $(y_{\rm op} - y_{\rm uw})\ (y_{\rm uw} - y_{\rm dw}) \le 0$ (*i.e.* when $y_{\rm uw}$ is a local extremum), the projection of $y_{\rm dw}$ onto I_σ is $y_{\rm uw}$ (so, as usual in this case, the scheme boils down to the upwind scheme).

3. Alternate directions algorithms

The alternate direction algorithm that we now present may be implemented for for $d = 2$ or 3; it is based on the use, in each direction, of one of the one-dimensional scheme presented in the previous section. We denote by $\mathcal{M}$ a structured mesh, *i.e.* a set of rectangles or cuboids (the cells), themeselves denoted by K. For $K \in \mathcal{M}$, let $\mathcal{E}^{(1)}(K)$, $\mathcal{E}^{(2)}(K)$ and $\mathcal{E}^{(3)}(K)$ be the faces of K perpendicular to the first, second and third axis of coordinates, respectively, and let $\mathcal{E}(K) = \cup_{1\le i\le d}\mathcal{E}^{(i)}(K)$. Let us present the algorithm for $d = 3$. Assuming that we perform first the transport in the first direction, then the second one and finally the third one, let us denote by y, $y^{(1)}$, $y^{(2)}$ and y^{n+1} the unknown at the beginning of the step, after the first transport step, after the second transport step and at the end of the time-step, respectively. We choose the conservative version of the algorithm given in the introduction; hence, setting $y^{(0)} = y$ and we use a discrete analogue of the following relation, for $i = 1, \dots, d$.

$$\frac{1}{\delta t}\,(y^{(i)} - y^{(i-1)}) + \operatorname{div}(y^{(i-1)}\boldsymbol{u}^{(i)}) - y\operatorname{div}(\boldsymbol{u}^{(i)}) = 0, \tag{10}$$

with $\boldsymbol{u}^{(i)} = (0, \dots, u_i, \dots)^t$. Summing over the steps, the last term in this relation vanishes since $\operatorname{div}(\boldsymbol{u}) = 0$, and so the scheme is indeed written in conservative form. We show in this section that, in addition, we can hope (or enforce) a maximum principle for this scheme.

Adding the transport steps (10) for $i = 1, \dots, d$, setting $y^{n+1} = y^{(3)}$ and $y^{(0)} = y^n$, and discretizing the divergence terms yields (for $d = 2, 3$):

$$\text{for } K \in \mathcal{M}, \quad y_K^{n+1} = y_K^n + \frac{\delta t}{|K|}\sum_{i=1}^{d}\Big[\sum_{\sigma\in\mathcal{E}^{(i)}(K)} |\sigma|\ \big(y_K^n - y_\sigma^{(i)}\big)\ u_{K,\sigma}\Big], \tag{11}$$

where $u_{K,\sigma}$ stands for the normal velocity through the face σ outward the cell K and the face approximations $y_\sigma^{(i)}$ are given by one of the one-dimensional schemes presented in Section 2.

For $K \in \mathcal{M}$, we denote by $\mathcal{N}(K)$ the set containing K itself and the (four if $d = 2$ or six if $d = 3$ and K has no face on the boundary) cells sharing a face with K, and define $\mathcal{N}_2(K)$ as $\mathcal{N}_2(K) = \cup_{L\in\mathcal{N}(K)}\mathcal{N}(L)$ and $\mathcal{N}_3(K)$ as $\mathcal{N}_3(K) = \cup_{L\in\mathcal{N}_2(K)}\mathcal{N}(L)$. For $\mathcal{A} = \{a_i,\ 1 \le i \le m\} \subset \mathbb{R}$, $\operatorname{conv}\{a_1, \dots, a_m\}$ stands for the convex hull of $\mathcal{A}$ (*i.e.* the interval $[\min_{1\le i\le m} a_i,\ max_{1\le i\le m} a_i]$). We are now in position to state the following result.

Lemma 3.1. *We suppose that the one-dimensional scheme is such that, for $K \in \mathcal{M}$ and $\sigma \in \mathcal{E}(K)$, $\sigma = K|L$,*

$$\begin{aligned} &\text{if } u_{K,\sigma} \le 0,\ y_\sigma \in \operatorname{conv}\{y_K, y_L\},\\ &\exists \alpha_\sigma \in [0, \Gamma] \text{ such that } y_\sigma - y_K = \alpha_\sigma\,(y_K - y_{M_{K,\sigma}}) \text{ otherwise,}\end{aligned} \tag{12}$$

with $M_{K,\sigma}$ the opposite cell to L (with respect to K) and Γ a non-negative real number. Let us suppose that the following set of CFL-like conditions holds:

$$\frac{\delta t}{|K|}\Big(\sum_{\sigma\in\mathcal{E}(K)} |\sigma|\ u_{K,\sigma}^- + \Gamma\sum_{\sigma\in\mathcal{E}(K)} |\sigma|\ u_{K,\sigma}^+\Big) \le 1, \qquad \frac{\delta t}{|K|}\ (1+\Gamma)\sum_{\sigma\in\mathcal{E}(K)} |\sigma|\ u_{K,\sigma}^+ \le 1. \tag{13}$$

Then, for $K \in \mathcal{M}$, the values $(y_K^{n+1})_{K\in\mathcal{M}}$ defined by (11) satisfy $y_K^{n+1} \in \operatorname{conv}\{y_L,\ L \in \mathcal{N}_d(K)\}$.

Remark 3.2. Note that, if the velocity field is divergence-free (at the discrete level), *i.e.*

$$\sum_{\sigma\in\mathcal{E}(K)} |\sigma|\ u_{K,\sigma} = 0,$$

the second assumption in (13) is implied by the first one.

Proof. **Two-dimensional case** – We first prove this lemma in the two-dimensional case. We have shown in Section 2.3 that, for $K \in \mathcal{M}$, $y_K^{(1)}$ is a convex combination of the left and right cells to K. We recall the expression of the scheme, omitting the superscript n for the unknowns at time t_n:

$$\text{for } K \in \mathcal{M}, \quad y_K^{n+1} = y_K + \frac{\delta t}{|K|}\Big[\sum_{\sigma \in \mathcal{E}^{(1)}(K)} |\sigma| \ \big(y_K - y_\sigma\big) \ u_{K,\sigma} + \sum_{\sigma \in \mathcal{E}^{(2)}(K)} |\sigma| \ \big(y_K - y_\sigma^{(1)}\big) \ u_{K,\sigma}\Big].$$

Let us denote by $T^{(2)}$ the last term and write

$$T^{(2)} = \sum_{\sigma \in \mathcal{E}^{(2)}(K)} |\sigma| \ \big(y_K - y_\sigma^{(1)}\big) \ u_{K,\sigma} = \sum_{\sigma \in \mathcal{E}^{(2)}(K)} |\sigma| \ \big(y_\sigma^{(1)} - y_K\big) \ u_{K,\sigma}^- + T^{(2),+},$$

with

$$T^{(2),+} = \sum_{\sigma \in \mathcal{E}^{(2)}(K)} |\sigma| \ \big(y_K - y_\sigma^{(1)}\big) \ u_{K,\sigma}^+.$$

This latter term equivalently reads:

$$T^{(2),+} = \sum_{\sigma \in \mathcal{E}^{(2)}(K)} |\sigma| \ \big(y_K - y_K^{(1)}\big) \ u_{K,\sigma}^+ + \sum_{\sigma \in \mathcal{E}^{(2)}(K)} |\sigma| \ \big(y_K^{(1)} - y_\sigma^{(1)}\big) \ u_{K,\sigma}^+.$$

By assumption (12), there exists $\alpha_\sigma \in [0, \Gamma]$ and $M_{K,\sigma} \in \mathcal{N}(K)$ such that $y_K^{(1)} - y_\sigma^{(1)} = \alpha_\sigma \ (y_{M_{K,\sigma}}^{(1)} - y_K^{(1)})$. We thus get

$$\begin{aligned} T^{(2),+} &= \sum_{\sigma \in \mathcal{E}^{(2)}(K)} |\sigma| \ \big(y_K - y_K^{(1)}\big) \ u_{K,\sigma}^+ + \sum_{\sigma \in \mathcal{E}^{(2)}(K)} |\sigma| \ \alpha_\sigma \ \big(y_{M_{K,\sigma}}^{(1)} - y_K^{(1)}\big) \ u_{K,\sigma}^+ \\ &= \Big[\sum_{\sigma \in \mathcal{E}^{(2)}(K)} |\sigma| \ (1 + \alpha_\sigma) \ u_{K,\sigma}^+ \Big] \ \big(y_K - y_K^{(1)}\big) + \sum_{\sigma \in \mathcal{E}^{(2)}(K)} |\sigma| \ \alpha_\sigma \ \big(y_{M_{K,\sigma}}^{(1)} - y_K\big) \ u_{K,\sigma}^+. \\ &= \frac{|K|}{\delta t} \ \nu_K^{(2),+} \ \big(y_K - y_K^{(1)}\big) + \sum_{\sigma \in \mathcal{E}^{(2)}(K)} |\sigma| \ \alpha_\sigma \ \big(y_{M_{K,\sigma}}^{(1)} - y_K\big) \ u_{K,\sigma}^+, \end{aligned}$$

with

$$\nu_K^{(2),+} = \frac{\delta t}{|K|} \sum_{\sigma \in \mathcal{E}^{(2)}(K)} |\sigma| \ (1 + \alpha_\sigma) \ u_{K,\sigma}^+.$$

By the second assumption in (13), we have $\nu_K^{(2),+} \leq 1$.
Finally, the scheme yields

$$y_K - y_K^{(1)} = -\frac{\delta t}{|K|} \sum_{\sigma \in \mathcal{E}^{(1)}(K)} |\sigma| \ \big(y_K - y_\sigma\big) \ u_{K,\sigma}.$$

and we may thus recast $T^{(2),+}$ as

$$T^{(2),+} = -\nu_K^{(2),+} \sum_{\sigma \in \mathcal{E}^{(1)}(K)} |\sigma| \ \big(y_K - y_\sigma\big) \ u_{K,\sigma} + \sum_{\sigma \in \mathcal{E}^{(2)}(K)} |\sigma| \ \alpha_\sigma \ \big(y_{K,\sigma}^{(1)} - y_K\big) \ u_{K,\sigma}^+, \tag{14}$$

Gathering the terms, we get

$$\begin{aligned} y_K^{n+1} = y_K + \frac{\delta t}{|K|}\Big((1 - \nu_K^{(2),+}) \sum_{\sigma \in \mathcal{E}^{(1)}(K)} |\sigma| \ \big(y_K - y_\sigma\big) \ u_{K,\sigma} \\ + \sum_{\sigma \in \mathcal{E}^{(2)}(K)} |\sigma| \ \big(y_\sigma^{(1)} - y_K\big) \ u_{K,\sigma}^- + \sum_{\sigma \in \mathcal{E}^{(2)}(K)} |\sigma| \ \alpha_\sigma \ \big(y_{K,\sigma}^{(1)} - y_K\big) \ u_{K,\sigma}^+ \Big). \end{aligned}$$

Using once again the assumption (12) on the one-dimensional scheme, we obtain, still with the coefficients $\alpha_\sigma \in [0,\Gamma]$ and the cell $M_{K,\sigma}$ adjacent to K,

$$y_K^{n+1} = y_K + \frac{\delta t}{|K|}\Big((1-\nu_K^{(2),+}) \sum_{\sigma\in\mathcal{E}^{(1)}(K)} |\sigma|\ \big(y_\sigma - y_K\big)\ u_{K,\sigma}^- \\ + (1-\nu_K^{(2),+}) \sum_{\sigma\in\mathcal{E}^{(1)}(K)} |\sigma|\ \alpha_\sigma\ \big(y_{M_{K,\sigma}} - y_K\big)\ u_{K,\sigma}^+ \\ + \sum_{\sigma\in\mathcal{E}^{(2)}(K)} |\sigma|\ \big(y_\sigma^{(1)} - y_K\big)\ u_{K,\sigma}^- + \sum_{\sigma\in\mathcal{E}^{(2)}(K)} |\sigma|\ \alpha_\sigma\ \big(y_{M_{K,\sigma}}^{(1)} - y_K\big)\ u_{K,\sigma}^+\Big).$$

Thanks to the properties of the one-dimensional scheme, $y_{M_{K,\sigma}}^{(1)} \in \mathrm{conv}\{y_L,\ L\in\mathcal{N}_2(K)\}$ and so does $y_\sigma^{(1)}$, and $y_\sigma \in \mathrm{conv}\{y_L,\ L\in\mathcal{N}(K)\}$. We thus obtain that $y_K^{n+1} \in \mathrm{conv}\{y_L,\ L\in\mathcal{N}_2(K)\}$ if the coefficient of y_K is non-negative, *i.e.*

$$\frac{\delta t}{|K|}\Big((1-\nu_K^{(2),+}) \sum_{\sigma\in\mathcal{E}^{(1)}(K)} |\sigma|\ u_{K,\sigma}^- + (1-\nu_K^{(2),+}) \sum_{\sigma\in\mathcal{E}^{(1)}(K)} |\sigma|\ \alpha_\sigma\ u_{K,\sigma}^+ \\ + \sum_{\sigma\in\mathcal{E}^{(2)}(K)} |\sigma|\ u_{K,\sigma}^- + \sum_{\sigma\in\mathcal{E}^{(2)}(K)} |\sigma|\ \alpha_\sigma\ \ u_{K,\sigma}^+\Big) \le 1,$$

which is a consequence of the first assumption in (13).

Three-dimensional case – The scheme now reads:

$$\text{for } K\in\mathcal{M},\quad y_K^{n+1} = y_K + \frac{\delta t}{|K|}\Big[\sum_{\sigma\in\mathcal{E}^{(1)}(K)} |\sigma|\ \big(y_K - y_\sigma\big)\ u_{K,\sigma} \\ + \sum_{\sigma\in\mathcal{E}^{(2)}(K)} |\sigma|\ \big(y_K - y_\sigma^{(1)}\big)\ u_{K,\sigma} + \sum_{\sigma\in\mathcal{E}^{(3)}(K)} |\sigma|\ \big(y_K - y_\sigma^{(2)}\big)\ u_{K,\sigma}\Big]. \quad (15)$$

We denote by T_3 the last summation in the brackets of the RHS, and again distiguish in the sum the upwind and downwind faces of K:

$$T_3 = \sum_{\sigma\in\mathcal{E}^{(3)}(K)} |\sigma|\ \big(y_\sigma^{(2)} - y_K\big)\ u_{K,\sigma}^- + T_3^+, \quad \text{with } T_3^+ = \sum_{\sigma\in\mathcal{E}^{(3)}(K)} |\sigma|\ \big(y_K - y_\sigma^{(2)}\big)\ u_{K,\sigma}^+.$$

Note that the proof for the two-dimensional case implies that $y_\sigma^{(2)} \in \mathcal{N}_2(K)$. By a similar computation as that of the case $d=2$, we obtain

$$T_3^+ = \frac{|K|}{\delta t}\ \nu_K^{(3),+}\ \big(y_K - y_K^{(2)}\big) + \sum_{\sigma\in\mathcal{E}^{(2)}(K)} |\sigma|\ \alpha_\sigma\ \big(y_{M_{K,\sigma}}^{(2)} - y_K\big)\ u_{K,\sigma}^+,$$

with

$$\nu_K^{(3),+} = \frac{\delta t}{|K|} \sum_{\sigma\in\mathcal{E}^{(3)}(K)} |\sigma|\ (1+\alpha_\sigma)\ u_{K,\sigma}^+, \qquad \nu_K^{(3),+} \le 1.$$

We now use the second step of the alternate direction scheme, which reads

$$y_K - y_K^{(2)} = -\frac{\delta t}{|K|}\Big[\sum_{\sigma\in\mathcal{E}^{(1)}(K)} |\sigma|\ \big(y_K - y_\sigma\big)\ u_{K,\sigma} \sum_{\sigma\in\mathcal{E}^{(2)}(K)} |\sigma|\ \big(y_K - y_\sigma^{(1)}\big)\ u_{K,\sigma}\Big],$$

to obtain that, returning to (15),

$$\text{for } K \in \mathcal{M}, \quad y_K^{n+1} = y_K + \frac{\delta t}{|K|}\Big[(1-\nu_K^{(3),+}) \sum_{\sigma\in\mathcal{E}^{(1)}(K)} |\sigma|\ \big(y_K - y_\sigma\big)\ u_{K,\sigma}$$
$$+ (1-\nu_K^{(3),+}) \sum_{\sigma\in\mathcal{E}^{(2)}(K)} |\sigma|\ \big(y_K - y_\sigma^{(1)}\big)\ u_{K,\sigma}$$
$$+ \sum_{\sigma\in\mathcal{E}^{(3)}(K)} |\sigma|\ \big(y_\sigma^{(2)} - y_K\big)\ u_{K,\sigma}^- + \sum_{\sigma\in\mathcal{E}^{(2)}(K)} |\sigma|\ \alpha_\sigma\ \big(y_{M_{K,\sigma}}^{(2)} - y_K\big)\ u_{K,\sigma}^+ \cdot\Big].$$

The end of the proof follow the same aruments as that of the two-dimensional case. □

Lemma 3.1 may be applied to the schemes presented in Section 2 as follows:

- The MUSCL scheme satisfies the assumptions of Lemma 3.1 with $\Gamma = 1$.
- Unfortunately, the other algorithms do not. However, we may derive schemes yielding conservative aternate-directions algorithms enjoying a discrete maximum principle by restricting the admissible interval for the face value, *i.e.* projecting it at the end of the process onto an interval of the form

$$I_{\sigma,\Gamma} = \mathcal{I}\big(y_{\rm uw},\ y_{\rm uw} + \Gamma\ (y_{\rm uw} - y_{\rm op})\big).$$

  This limitation may be made less and less restrictive by taking larger and larger values of Γ, at the price of a restriction of the admissible time step, to respect the constraints (13). Note also that, for the algorithms of Section 2.3, with the notations of Lemma 3.1, we have

$$\alpha_\sigma \le \frac{1-\nu_\sigma}{\nu_\sigma}, \quad \nu_\sigma = \frac{|\sigma|\ u_{K,\sigma}\ \delta t}{|K|}.$$

  A straightforward computation shows that we thus get a relation of the form (14) with

$$\nu_K^{(2),+} = \sum_{\sigma\in\mathcal{E}^{(2)}(K)} \beta_\sigma, \quad \beta_\sigma \le 1.$$

  The coefficient $\nu_K^{(2),+}$ is then smaller than 1 as soon as the number of outflow faces in the cell K for the velocity $(0, u_2)^t$ does not exceed 1, that is, in other words, if the second component of the velocity does not change of sign in K. Otherwise, $\nu_K^{(2),+}$ may be greater than 1, and the proof fails. However, if the velocity field is regular, convective fluxes in this case will be low, and under- and over-shoots, if any, should be of reduced amplitude.

4. Numerical tests

We present in this section a series of numerical tests. Since, for all the proposed schemes, the approximation of the unknown at the face is a convex combination of the unknown in the neighbour cells, the consistency of the schemes in the Lax-Wendroff sense [12] is clear (see *e.g.* [6] for a proof on general meshes), and checking the first-order convergence when the space and time steps tends to zero is of poor interest; therefore, we focus here on the quality of the solution for a given (and rather coarse) mesh. These tests consists in transporting a characteristic function of an initially given domain, which is the initial support of y, denoted by $S_y(t)$ (so $y(\boldsymbol{x}, 0) = 1$ if $\boldsymbol{x} \in S_y(0)$ and $y(\boldsymbol{x}, 0) = 0$ otherwise), and we discuss three specific issues: the preservation of the bounds for y, the scheme diffusion and the eventual spurious numerical shape deformations of $S_y(t)$.

In the four following sections, we systematically compare four schemes which differ by the underlying one-dimensional discretization, *i.e.* the scheme used for the one-dimensional transport steps: the standard first-order upwind and MUSCL approximations, the THINC scheme and the anti-diffusive scheme. For the

THINC scheme, we always choose $\beta = 2$ for the reconstruction function. We first address the transport of a square and a circle characteristic function at a constant skew-to-the-mesh velocity (Section 4.1) and by a uniform rotation (Section 4.2). These two flows enjoy the property that the sub-step velocities $(u_x, 0)^t$ and $(0, u_y)^t$ are divergence-free, so the maximum principle is ensured at each step of the alternate-directions algorithm. This is no more the case in the third test (Section 4.3), and the maximum principle preservation issue is addressed here. We conclude this study by a a test inspired from [14], where the $S_y(t)$ undergoes large changes (4.4); we assess here the effects of the generalization of the mesh: use of a non-uniform grid and of non-conforming local mesh refinement. The anti-diffusive schemes considered in this paper are not designed to transport regular functions; we briefly report such a test in the appendix (Section B), and indeed observe a poor behaviour.

We also mention that a one-dimensional computation has been performed with the anti-diffusive scheme, with $S_y(0) = (-0.5, 0.5)$ and $u = x$. We obtained the expected results: the scheme captures the discontinuity in a single cell (*i.e.* the unknown y takes a value different from 1 and 0 in only a cell for the two present discontinuities, travelling to the left and to the right respectively), and results are close to the analytical solution. Note that, in contrats to what happens with a constant velocity (see [5]), the scheme cannot compute the solution exactly because of the interpolation of the velocity; more precisely speaking, writing $u\,\partial_x y = \partial_x(u\,y) - \partial_x(u)\,y$, with a suitable evaluation of u, we may hape the flux $u\,y$ to be computed exactly (by construction of the scheme), but it is impossible for the production term $\partial_x(u)\,y$. Indeed, with an interpolation of u at the faces, the evaluation of the mean value of $\partial_x(u)$ over a cell K is exact, but

$$\frac{1}{|K|}\int_K \partial_x(u)\,y\;\mathrm{d}x \neq \Big(\frac{1}{|K|}\int_K \partial_x(u)\;\mathrm{d}x\Big)\;\;\Big(\frac{1}{|K|}\int_K y\;\mathrm{d}x\Big)$$

if y is not constant over K.

Computations are run with the open-source CALIF^{3}S software developed at IRSN [3].

4.1. **Transport by a constant skew-to-the-mesh velocity**

We begin this study by considering the transport by a constant velocity field:

$$\boldsymbol{u} = \begin{bmatrix} 1 \\ 1 \end{bmatrix}.$$

The computational domain is the unit square $\Omega = (0,1) \times (0,1)$, and the final time is $T = 0.6$. We use a uniform 100×100 mesh and the time step is $\delta t = 1/400$. As noted in the introduction of the section, the convective field for each transport step is divergence-free, so the alternate-directions algorithm preserves the maximum principle at each step (which is indeed observed).

Transport of the characteristic function of a square – We first consider the following initial condition:

$$y = 1 \text{ if } \boldsymbol{x} \in (0.1, 0.3) \times (0.1, 0.3),\;\; y = 0 \text{ otherwise.}$$

Results at $t = 0.6$ are given on Figure 4. Here, and throughout this numerical study, the blue and red colors correspond to $y = 0$ and $y = 1$, respectively; in addition, as in most of the following figures, we plot the solution only over a subdomain Ω_p of Ω including the support of y. The first-order upwind scheme is over-diffusive while the anti-diffusive scheme yields the exact solution. This latter behaviour is explained by the fact that the initial condition is exactly represented (because the boundary of the zone where $y = 1$ at $t = 0$ matches the cells edges), the final solution may also be exactly represented by the discretization (for the same reasons) and, by construction, the one-dimensional scheme performs an exact transport in these conditions. The jump of the solution slightly spreads with the THINC scheme, and the MUSCL scheme (which is not dedicated to the transport of step functions) is more diffusive. A complementary study, not presented here, shows that, with the THINC scheme, the discontinuity approximatively spreads over 2, 4 and 6 cells when the value of the parameter β governing the stiffness of the reconstuction takes the values 2, 1.5 and 1.25 respectively; for large values of β, one recovers the anti-diffusive scheme.

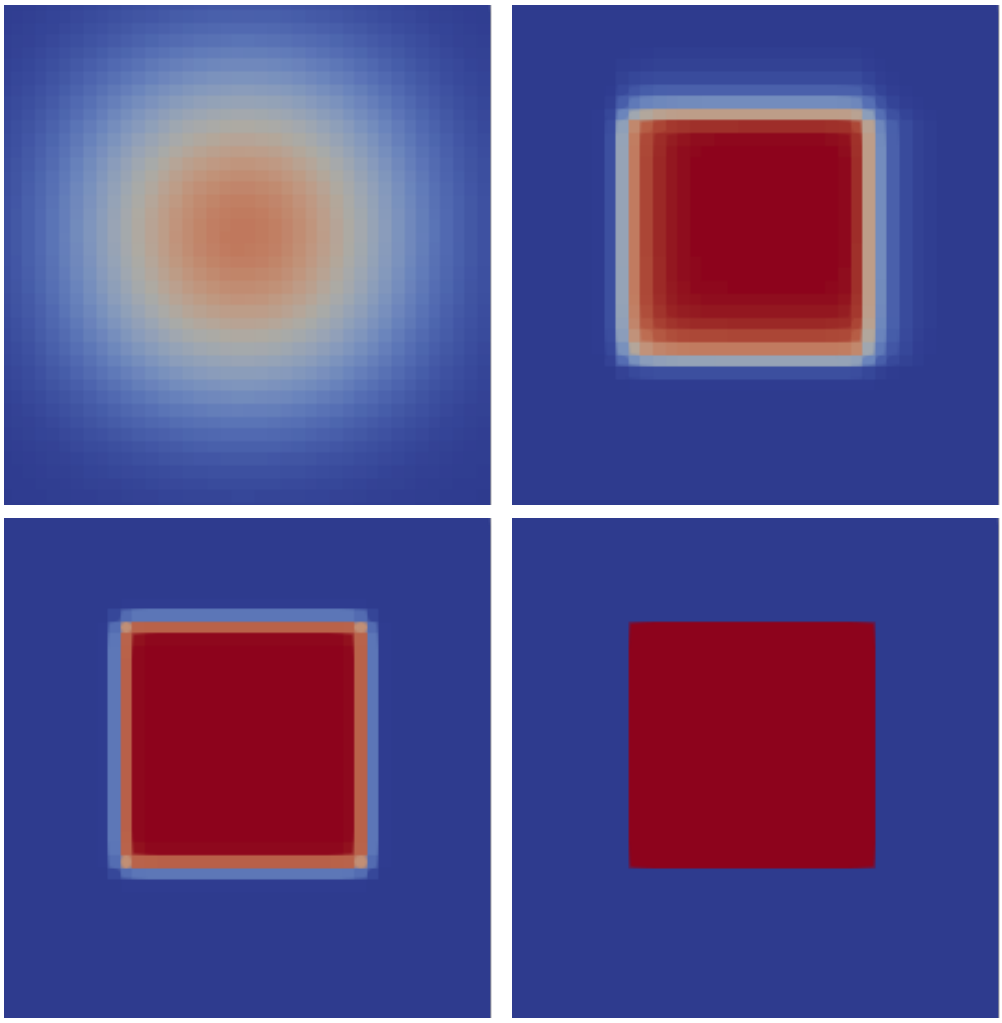

FIGURE 4. Translation of the characteristic function of a square – Results obtained at $t = 0.6$ with the alternate-directions algorithm based on the upwind scheme (top-left), the MUSCL scheme (top-right), the THINC scheme (bottom-left) and the anti-diffusive scheme (bottom-right). Only the top-left part of the computational domain is shown.

Transport of the characteristic function of a circle – We now consider the following initial condition:

$$y = 1 \text{ if } \left[(x_1 - 0.2)^2 + (x_2 - 0.2)^2\right]^{1/2} \leq 0.125, \ y = 0 \text{ otherwise.}$$

Results at $t = 0.6$ are given on Figure 5. Except of course the first-order upwind scheme, the other ones exhibit a compressive behaviour, which generate "angles" in the boundary of the support of y (note however that the scheme is initialized by taking in each cell the value at the mass-center, and not the average value, which already alters, to some extent, the regularity of the shape of the support). As a counterpart, one may expect that, at least with the THINC and the anti-diffusive scheme, the diffusion does not amplify with time, which is favourable for the long-term behaviour of the solution (see Figure 8 and the related discussion below). This property of the anti-diffusive scheme is more precisely characterized for the constant velocity one-dimensional transport in [5]: when starting from a smooth initial condition, the schemes first yields a solution exhibiting plateaus, with three cells in each plateau; then this solution is transported exactly.

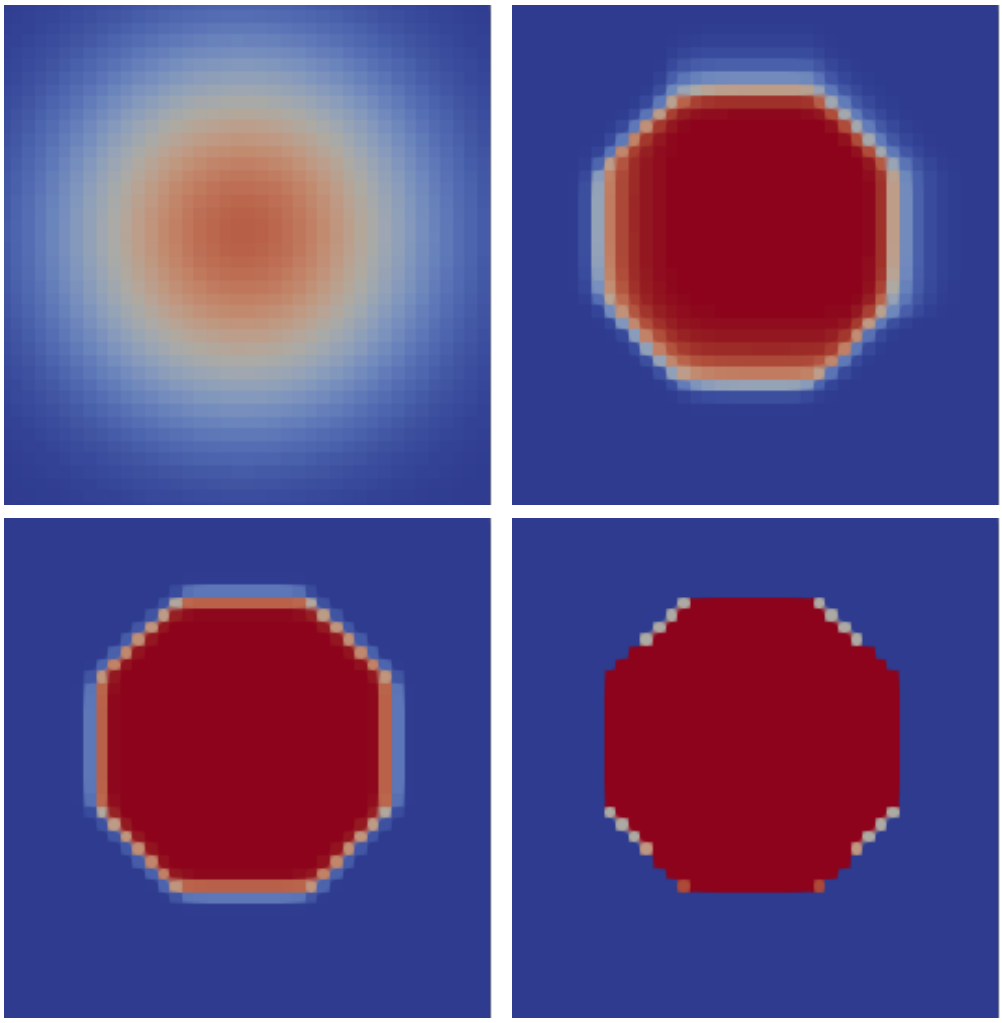

FIGURE 5. Translation of the characteristic function of a circle – Results obtained at $t = 0.6$ with the alternate-directions algorithm based on the upwind scheme (top-left), the MUSCL scheme (top-right), the THINC scheme (bottom-left) and the anti-diffusive scheme (bottom-right). Only the top-left part of the computational domain is shown.

4.2. **Uniform rotation**

We now consider a velocity field associated to a uniform rotation at an angular velocity equal to 1:

$$\boldsymbol{u} = \begin{bmatrix} x_2 \\ -x_1 \end{bmatrix}.$$

Once again, the velocity fields $\boldsymbol{u}^{(1)} = (x_2, 0)^t$ and $\boldsymbol{u}^{(2)} = (0, -x_1)^t$ are both divergence-free (in fact, they correspond to a free-shear flow), and each transport step preserves the solution bounds. The computational domain is $\Omega = (-1, 1) \times (-1, 1)$, and the final time is $2\,\pi$, so the final exact solution is equal to the initial condition. We use a uniform 200×200 mesh, and the time step is equal to $\delta t = 1/400$. We consider two initial conditions, the characteristic function of a square (□) and of a circle (○):

(□) $y = 1$ if $\boldsymbol{x} \in (-0.2, 0.2) \times (0.45, 0.85)$, $y = 0$ otherwise,

(○) $y = 1$ if $\left[(x_1 - 0.25)^2 + (x_2 - 0.75)^2\right]^{1/2} \leq 0.2$, $y = 0$ otherwise.

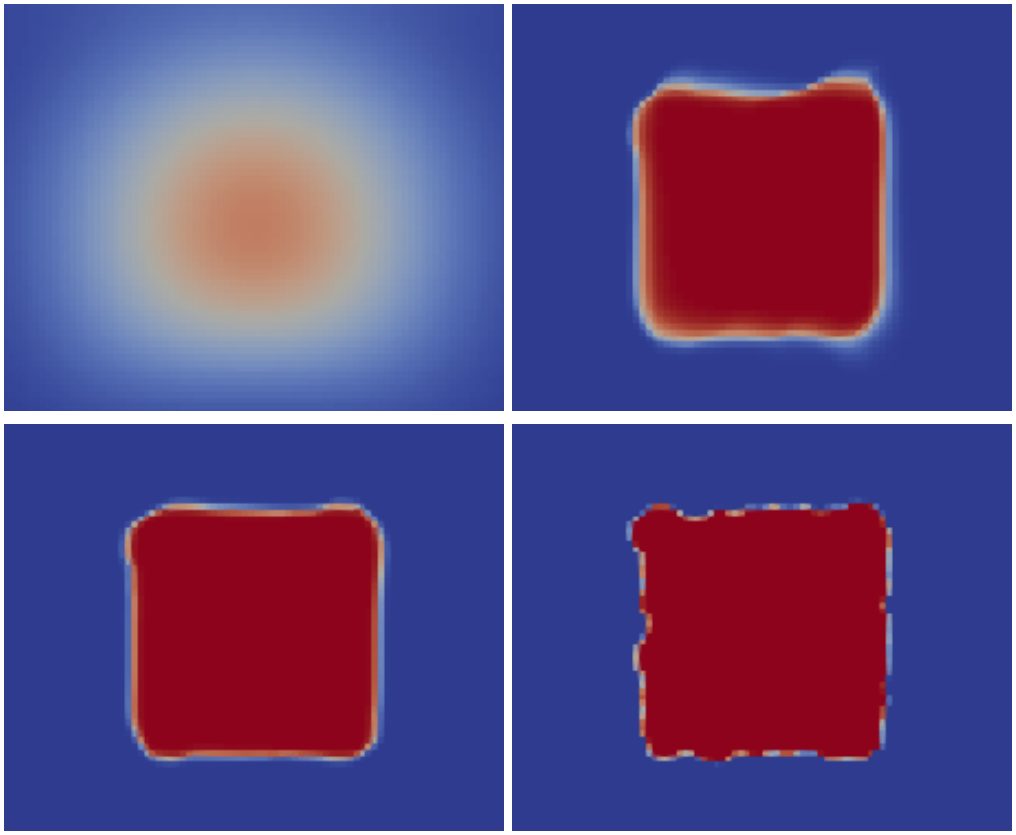

FIGURE 6. Rotation of the characteristic function of a square – Results obtained at $t = 2\,\pi$ with the alternate-directions algorithm based on the upwind scheme (top-left), the MUSCL scheme (top-right), the THINC scheme (bottom-left) and the anti-diffusive scheme (bottom-right). Only the top-middle part of the computational domain is shown.

Results at $t = 2\,\pi$ (so after a complete rotation) are given on Figures 6 and 7. Once again, we observe a very low diffusion for the THINC scheme and an absence of diffusion with the anti-diffusive scheme, at the price of the onset of some irregularities in the shape of $S_y(2\,\pi)$, more pronounced for the latter scheme. To assess the long-time behaviour of the solution, we show on Figure 8 the solution obtained with the THINC scheme after several complete rotations with the initial condition ($\circ$); we observe that the diffusion is completely controlled, but the shape $S_y(t)$ is progressively altered.

4.3. **Transport by a straining velocity field**

We now consider the following velocity field:

$$\boldsymbol{u} = \begin{bmatrix} x_1 \\ -x_2 \end{bmatrix}.$$

This velocity field corresponds to a stretching in the first direction and a compression in the second one, and the divergence of the convective field at each transport step is different from zero: $\mathrm{div}(u_1, 0)^t = 1$, $\mathrm{div}(0, u_2)^t = -1$. The alternate-directions algorithm is thus likely to generate under- and over-shoots.

The computational domain is $\Omega = (0, 1) \times (0, 1)$, and we use a 100×100 uniform mesh. The time step is $\delta t = 1/400$.

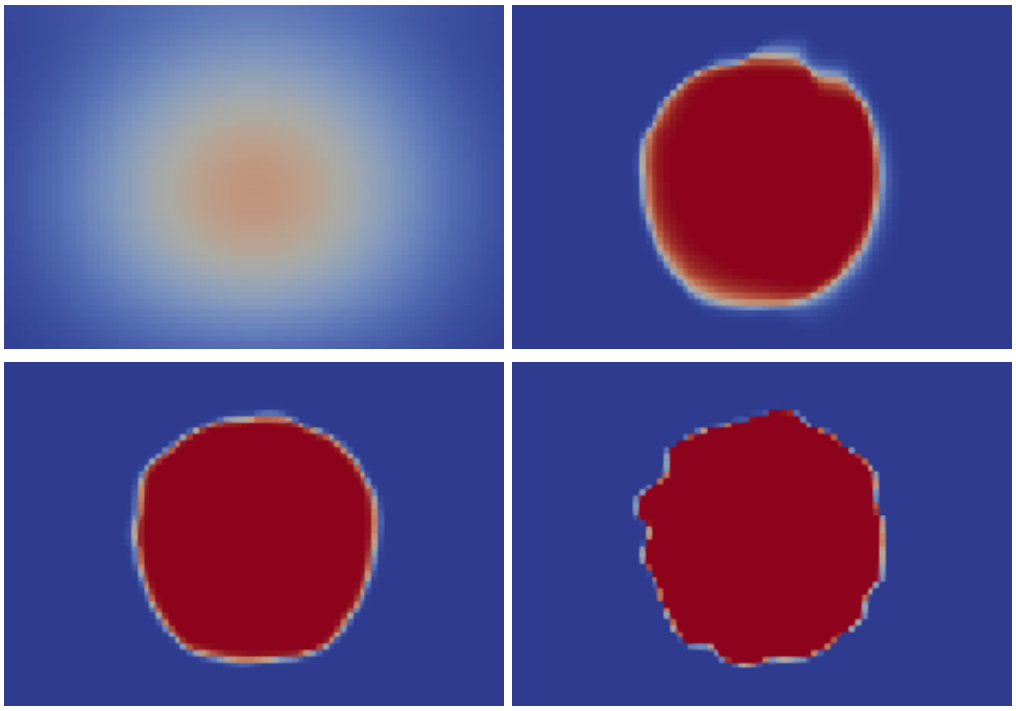

FIGURE 7. Rotation of the characteristic function of a circle – Results obtained at $t = 2\,\pi$ with the alternate-directions algorithm based on the upwind scheme (top-left), the MUSCL scheme (top-right), the THINC scheme (bottom-left) and the anti-diffusive scheme (bottom-right). Only the top-middle part of the computational domain is shown.

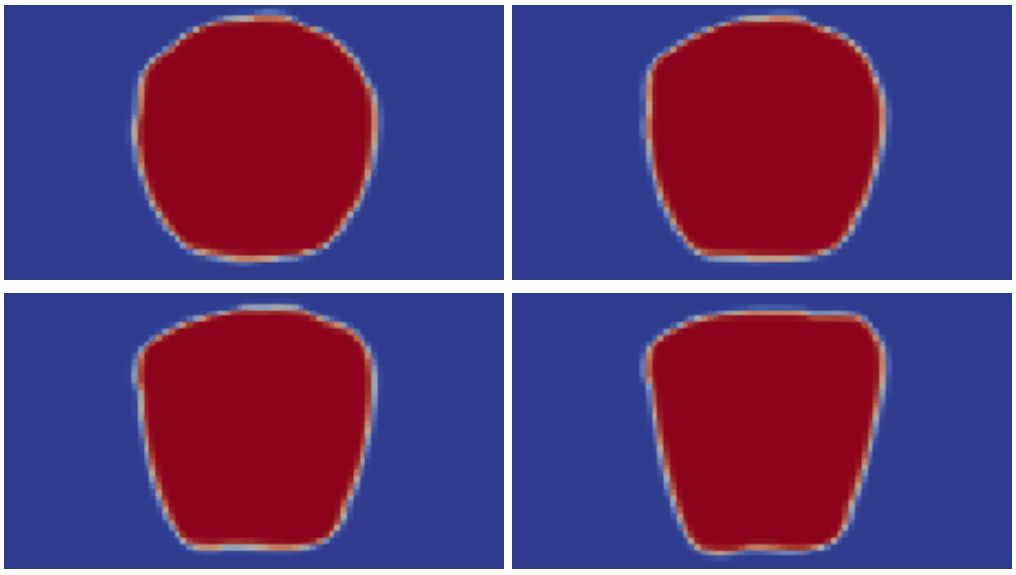

FIGURE 8. Rotation of the characteristic function of a circle – Results obtained with the alternate-directions algorithm based on the THINC scheme after one (bottom-left), two (top-right), four (bottom-left) and eight (bottom-right) rotations. Only the top-middle part of the computational domain is shown.

We consider two initial conditions, the characteristic function of a rectangle (□) and of a circle (○):

$$(\square) \qquad y = 1 \text{ if } \boldsymbol{x} \in (0.05, 0.15) \times (0.6, 0.9),\ y = 0 \text{ otherwise,}$$

$$(\circ) \qquad y = 1 \text{ if } \left[(x_1 - 0.15)^2 + (x_2 - 0.8)^2\right]^{1/2} \leq 0.125,\ y = 0 \text{ otherwise.}$$

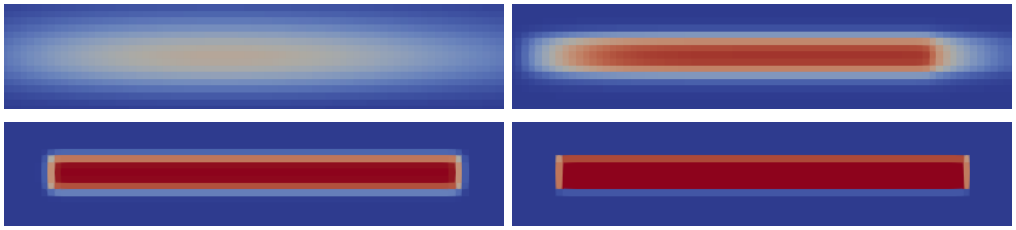

FIGURE 9. Motion of the characteristic function of a rectangle in a straining velocity field – Results obtained at $t = 1.8$ with the alternate-directions algorithm based on the upwind scheme (top left), the MUSCL scheme (top right), the THINC scheme (bottom left) and the anti-diffusive scheme (bottom right). The blue and red colors correspond to $y = 0$ and $y = 1$, repectively. Only the bottom part of the domain is shown.

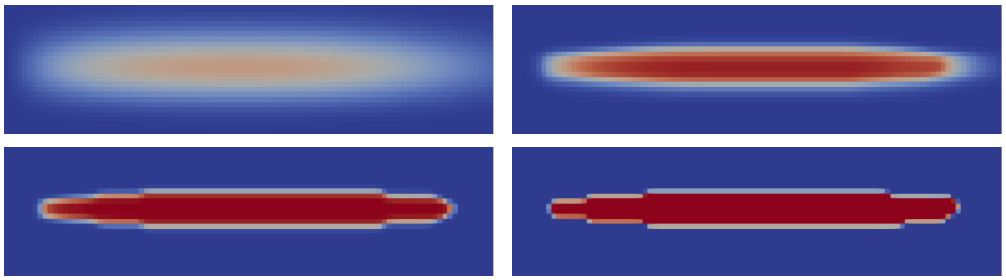

FIGURE 10. Motion of the characteristic function of a circle in a straining velocity field – Results obtained at $t = 1.8$ with the alternate-directions algorithm based on the upwind scheme (top left), the MUSCL scheme (top right), the THINC scheme (bottom left) and the anti-diffusive scheme (bottom right). The blue and red colors correspond to $y = 0$ and $y = 1$, repectively. Only the bottom part of the domain is shown.

Results at $t = 1.8$, for the initial condition ($\square$), and $t = 1.25$, for the initial condition ($\circ$), are given on Figure 9 and Figure 10 respectively. They confirm the diffusive (or anti-diffusive) properties of the discretizations observed in the previous sections, together with (slight) deformations of the support of y due to their compressive behaviour. In addition, we observe in the computations that all the schemes except the anti-diffusive one satisfie a discrete maximum principle. We thus test for this latter discretization the *a posteriori* limitation suggested by the analysis of Section 3; results for various values of the parameter Γ are reported on Figure 11 and 12. The under- and over-shoots are characterized as follows: at each time step, we record the minimum and maximum value of the solution, and then clip the solution in the $[0, 1]$ interval. Without any *a posteriori* limitation, the observed minimum value is $-7.\,10^{-5}$ for the initial condition ($\square$), and -0.0001 for the initial condition ($\circ$); For $\Gamma = 4$, these values are reduced to $-4.\,10^{-6}$ and $-5.\,10^{-5}$ respectively, and no under- or over-shoot is observed for lower values of Γ. Since no significant diffusion is visible on Figures 11 and 12 for $\Gamma = 3$ or $\Gamma = 2$, it seems that combining the anti-diffusive discretization with an *a posteriori* limitation yields a both accurate and stable scheme.

4.4. **A test with large topological changes**

In this section, we conclude the study by a test inspired by [4]. The computational domain is $\Omega = (0, \pi) \times (0, \pi)$. The velocity field reads:

$$\boldsymbol{u} = \begin{bmatrix} \sin(x_1)\,\cos(x_2) \\ -\cos(x_1)\,\sin(x_2) \end{bmatrix}, \tag{16}$$

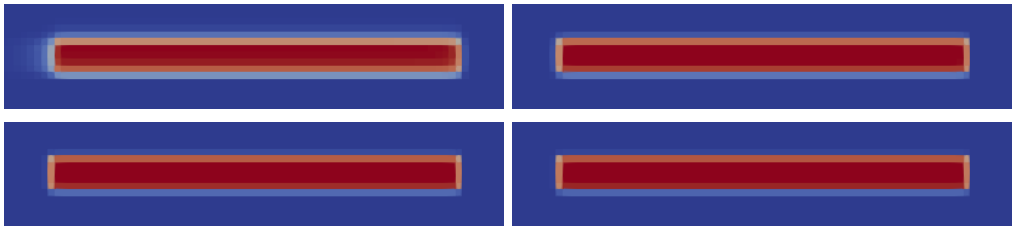

FIGURE 11. Motion of the characteristic function of a rectangle in a straining velocity field – Results obtained at $t = 1.8$ with the alternate-directions algorithm based on the anti-diffusive scheme and an additional limitation with $\Gamma = 1$ (top left), $\Gamma = 2$ (top right), $\Gamma = 3$ (bottom left) and $\Gamma = 4$ (bottom right). The blue and red colors correspond to $y = 0$ and $y = 1$, repectively. Only the bottom part of the domain is shown

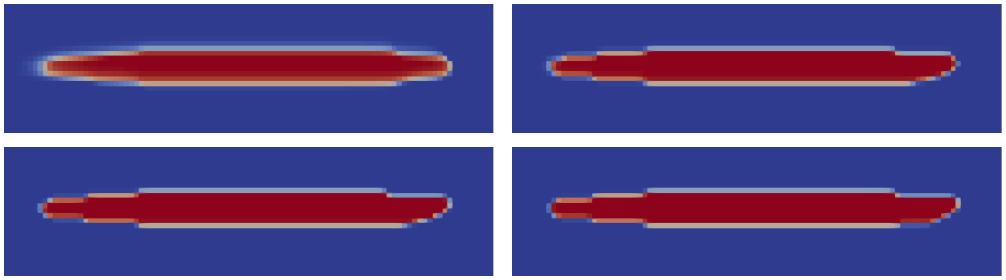

FIGURE 12. Motion of the characteristic function of a circle in a straining velocity field – Results obtained at $t = 1.8$ with the alternate-directions algorithm based on the anti-diffusive scheme and an additional limitation with $\Gamma = 1$ (top left), $\Gamma = 2$ (top right), $\Gamma = 3$ (bottom left) and $\Gamma = 4$ (bottom right). The blue and red colors correspond to $y = 0$ and $y = 1$, repectively. Only the bottom part of the domain is shown.

and the initial condition is the characteristic function of a circle:

$$y = 1 \text{ if } \left[(x_1 - \frac{\pi}{2})^2 + (x_2 - \frac{\pi+1}{5})^2\right]^{1/2} \leq \frac{\pi}{5},\ y = 0 \text{ otherwise.}$$

We first begin with obtaining a reference solution with a (fine) 512×512 mesh and a time-step $\delta t = \pi/(4 \times 512)$, up to $t = 11.5$. Results are sketched on Figure 13, and we observe that, with this initial condition and this velocity field, the support pf y undergoes large topological changes. Then we turn to a computation closer to the presented one in [4]: a (coarser) 128×128 mesh is chosen, the time-step is consequently set to the (larger) $\delta t = \pi/(4 \times 128)$ value, the velocity is kept to the value given by Equation (16) up to the time $T/2$ and then its sign is changed up to T, so the final solution should be equal to the initial one. From preliminary computations, we observe that this final state becomes poorly reproduced when, at the time when the flow is reversed, the thickness of the support of y is lower than the space step; indeed, in such a case, because of the compressive behaviour of the tested higher-order schemes, the support of y is fragmented by the discretization. This lead us to choose $T/2 = 7.67$. Results obtained at $t = T$ with the different schemes are shown on Figure 14; the anti-diffusive scheme is combined with an *a posteriori* limitation with $\Gamma = 2$ to ensure the maximum principle. These results confirm the observations of the previous sections.

We finally complete the study by testing the schemes on more general meshes. Figure 15 shows the results given by the THINC scheme with a non-uniform mesh, obtained as a grid based on two lists for the first and second coordinates of the vertical and horizontal faces, respectively. For the first (second) coordinate, this list is such that the x_1-size (x_2-size) of the left row (top line) of cells is 0.009 and the x_1-size (x_2-size) of the right row (bottom line) of cells is 0.05; in-between, the progression of the real numbers in these lists is geometrical. This lead to a number of cell equal to 17161, close to the numeber of cells of a 128×128 mesh

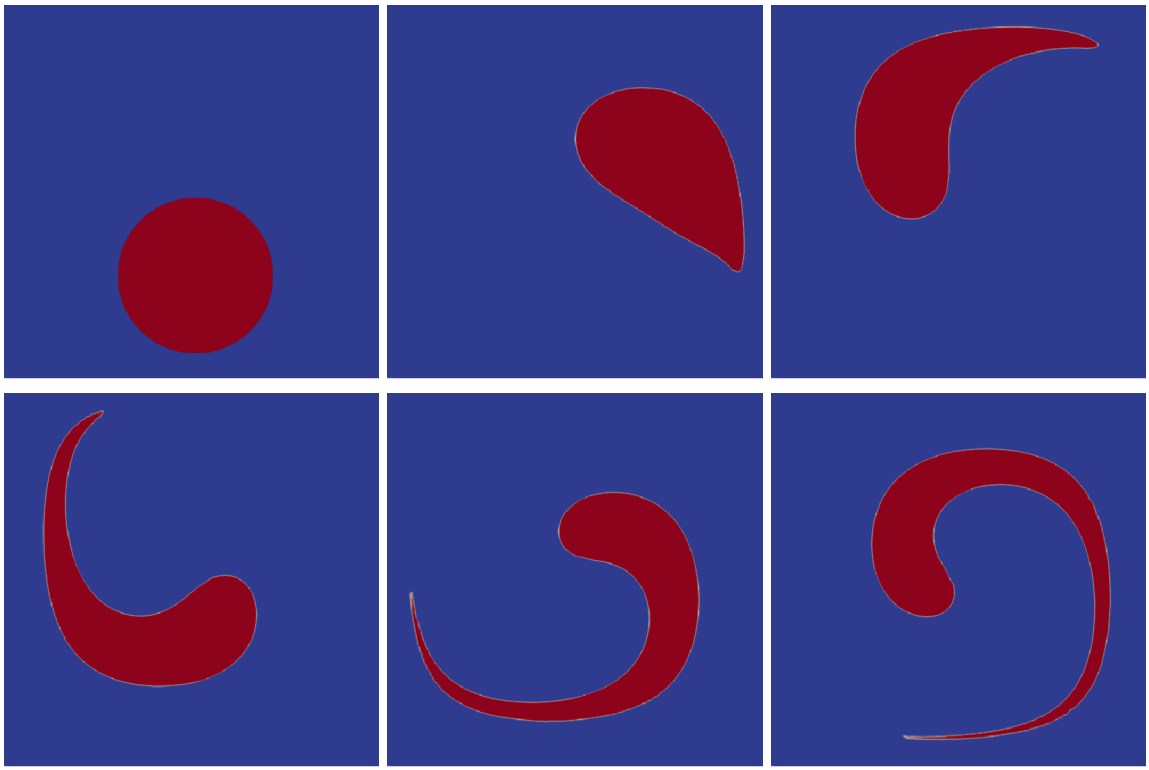

FIGURE 13. Characteristic function of a circle in a straining velocity field undergoing large topological changes – From top-left to bottom-right, initial condition, results obtained at $t = 0$, $t = 2.3$, $t = 4.6$, $t = 6.9$, $t = 9.2$ and $t = 11.5$ with the alternate-directions algorithm based on the THINC scheme.

(16384). The time step, governed by the smallest cells, is $\delta t = 0.004$. Result show a larger diffusion, due to the larger size of the largest cells, together with a more regular final shape of the support of y, probably due to the fact that the solution is better captured at times close to $T/2$, when the thinnest part of $S_y(t)$ lies in the refined zone of the mesh.

Finally, we may consider the alternate-directions algorithm as two consecutive transport steps, with $\boldsymbol{u} = (u_1, 0)^t$ and $\boldsymbol{u} = (0, u_2)^t$ respectively, whatever the mesh may be. This gives sense to the use of a locally refined mesh, obtained from a 50×50 uniform mesh by dividing by 4 the cells of the top-left quarter of the computational domain. Results are given on Figure 16; we do not observe any numerical artefact at the boundary between the refined and non-refined zones.

5. Conclusion

We first proposed in this paper an extension of the so-called Lagrange-projection algorithm (or downwind scheme with an Ultrabee limiter) [1, 5, 15] for the transport equation in one space dimension with a non-constant velocity; as its constant velocity counterpart, this scheme is designed to capture the discontinuities separating two plateaus in only one cell, and so is referred to as "anti-diffusive" throughout this paper. Then this scheme, together with the so-called THINC scheme [4], is embedded in an alternate-directions algorithm, to tackle the transport of characteristic functions in two and three space dimensions, on structured grids. For this problem, we introduce a conservative scheme and show that, possibly up to an additional flux limitation, this schemes satisfies a discrete maximum principle. Numerical tests show that the alternate-directions algorithm based on the anti-diffusive and, almost to a similar extent, on the THINC scheme are indeed able to transport characteristic functions with almost no diffusion. In addition, the THINC-based

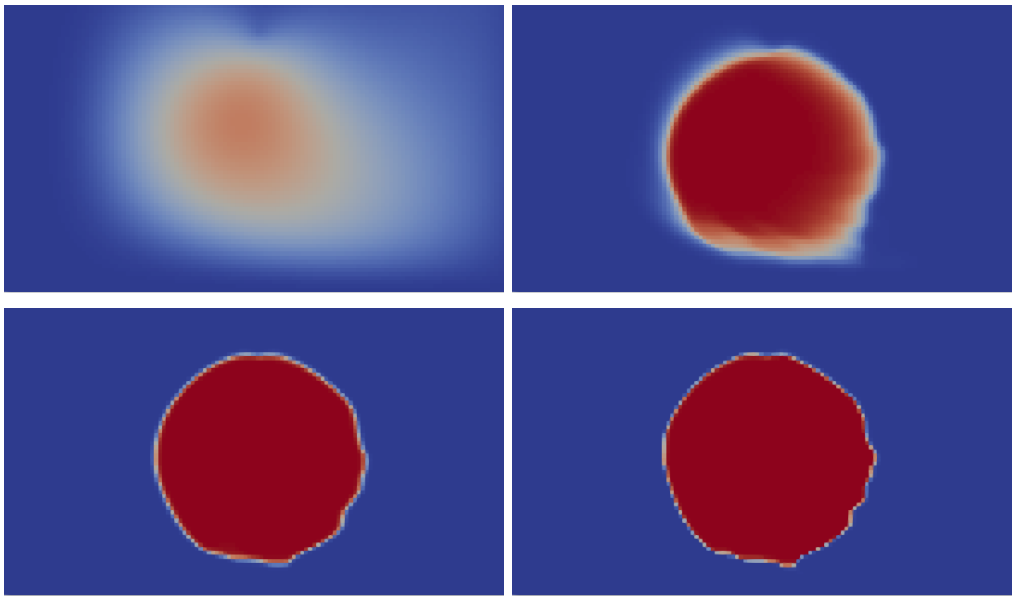

FIGURE 14. Characteristic function of a circle in a straining velocity field undergoing large topological changes – Final state obtained with the alternate-directions algorithm based on the upwind scheme (top left), the MUSCL scheme (top right), the THINC scheme (bottom left) and the anti-diffusive scheme limited with $\Gamma = 2$ (bottom right). Only the bottom part of the domain is shown.

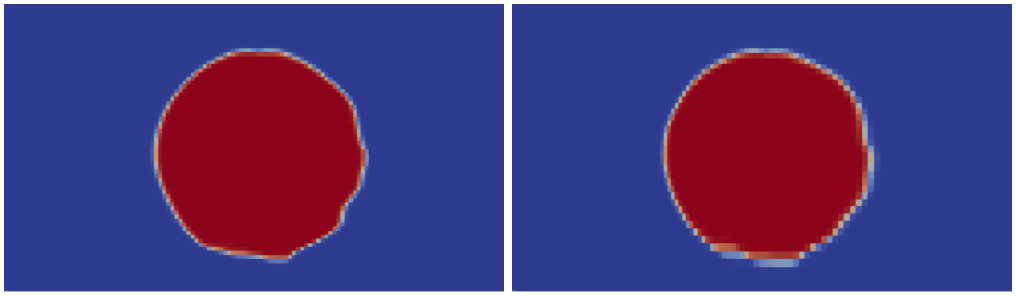

FIGURE 15. Characteristic function of a circle in a straining velocity field undergoing large topological changes – Final state obtained with the alternate-directions algorithm based on the THINC scheme, with a uniform (left) and non-uniform (right) mesh.

algorithm seems to satisfy the discrete maximum principle (this property is not proven here), while the anti-diffusive-based algorithm needs the above-mentioned additional flux limitation to satisfy the same property; however, this latter does not seem to generate any significant additional diffusion.

Both schemes seem thus to be good candidates to transport the phase indicator function in a Volume-Of-Fluid (VOF) approach, and such a solver is now under development in the CALIF^{3}S software at IRSN [3]. Extension to unstructured grids of the downwind-limited strategy, to minimize the numerical diffusion, is also underway.

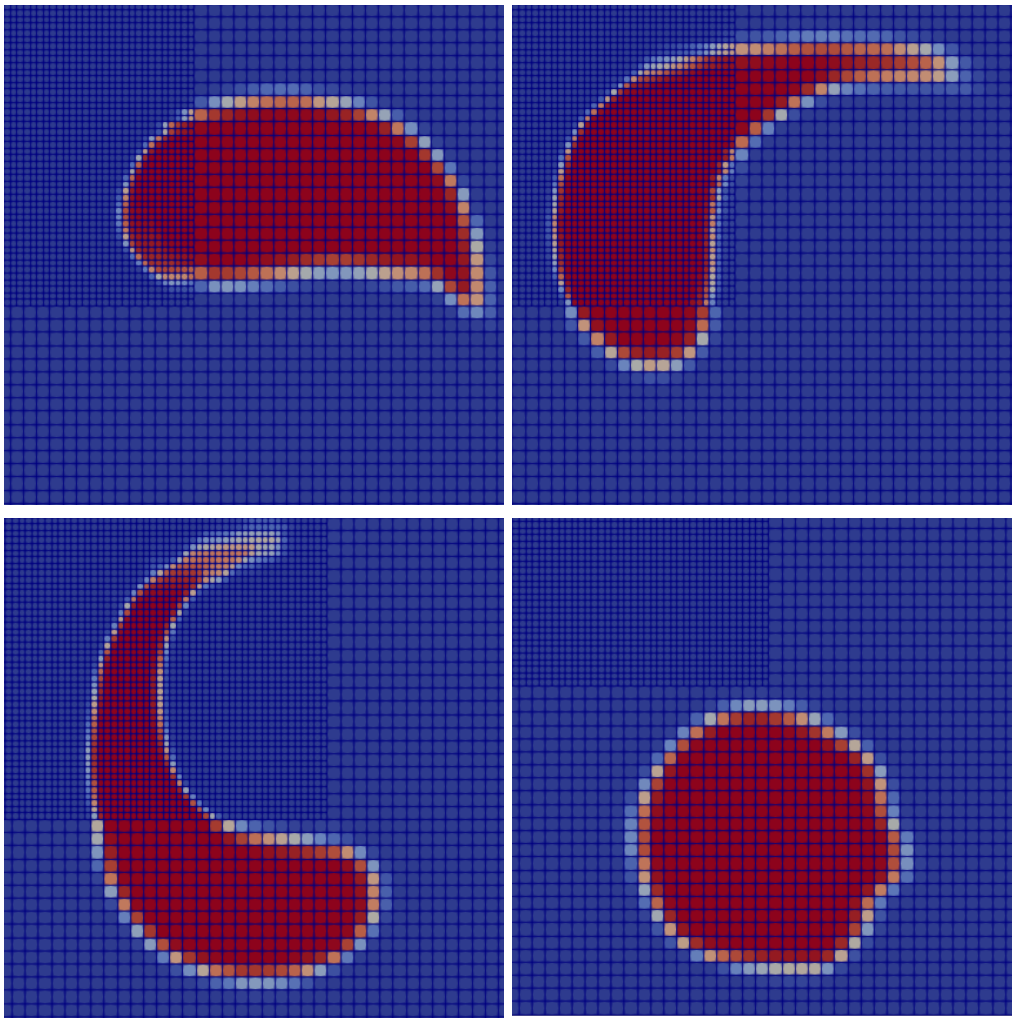

FIGURE 16. Characteristic function of a circle in a straining velocity field undergoing large topological changes – Results obtained at $t = 3.07$, $t = 4.61$, $t = 6.14$ and $t = 15.34$ (final state) with the alternate-directions algorithm based on the THINC scheme on a locally refined (non-conforming) mesh.

Appendix A. Reconstruction by a hyperbolic tangent

Let σ be a face of the (1D) mesh, y, y_+ and y_- the value of the unknown in the upwind cell K, the downwind cell and the neighbour of K on the opposite side of σ, respectively. Up to a change of coordinates, we may assume that $K = (0, 1)$, and that $\sigma = \{1\}$ (note that it means that we have possibly reoriented the axis and that the velocity at σ is non-negative). We suppose the following reconstruction of y in K:

$$\tilde{y}(x) = \bar{y} + \frac{\delta y}{2}\,\tanh\big(\beta(x - x_0)\big), \quad \text{with } \bar{y} = \frac{1}{2}\,(y_+ + y_-),\ \delta y = y_+ - y_-,$$

with x_0 to de determined in such a way that

$$\int_0^1 \tilde{y}(x)\ \mathrm{d}x = y. \tag{17}$$

We assume that $(y - y_-)(y_+ - y) > 0$ so x_0 exists; note however that x_0 may lie outside the interval $(0, 1)$ (for instance, y close to y_- yields a very large value for x_0). Thanks to the expression of $\tilde{y}$, we have:

$$\int_0^1 \tilde{y}(x)\ \mathrm{d}x = \bar{y} + \frac{\delta y}{2}\,\frac{1}{\beta}\,\Big[\ln\Big(\cosh\big(\beta(x - x_0)\big)\Big)\Big]_0^1.$$

Condition (17) easily yields

$$\frac{\cosh\big(\beta(1 - x_0)\big)}{\cosh(\beta x_0)} = \exp\Big(2\,\beta\ \frac{y - \bar{y}}{\delta y}\Big).$$

Let us denote by B the right-hand side of this relation. We get:

$$-\sinh(\beta)\ \tanh\big(\beta(1 - x_0)\big) = -\frac{1}{B}\frac{\sinh(\beta)\ \sinh\big(\beta(1 - x_0)\big)}{\cosh(\beta x_0)}$$

Thanks to the fact that the hyperbolic sinus and cosinus are impair and pair functions respectively, and thanks to the identity $\cosh(a + b) = \cosh(a)\ \cosh(b) + \sinh(a)\ \sinh(b)$, for $(a, b) \in \mathbb{R}^2$, we get

$$-\sinh(\beta)\ \tanh\big(\beta(1 - x_0)\big) = \frac{1}{B}\frac{\cosh(\beta x_0) - \cosh(\beta)\ \cosh\big(\beta(1 - x_0)\big)}{\cosh(\beta x_0)} = \frac{1}{B}\big(1 - \cosh(\beta)B\big).$$

This yields:

$$\tanh\big(\beta(1 - x_0)\big) = \frac{1}{\tanh(\beta)} - \frac{1}{\sinh(\beta)\ B}. \tag{18}$$

In some algorithms, the value at σ is defined as the value taken by the reconstruction at $x = 1$, *i.e.*

$$y_\sigma = \tilde{y}(1) = \bar{y} + \frac{\delta y}{2}\,\tanh\big(\beta(1 - x_0)\big).$$

so, finally,

$$y_\sigma = \bar{y} + \frac{\delta y}{2}\,\Big(\frac{1}{\tanh(\beta)} - \frac{1}{\sinh(\beta)\ B}\Big).$$

However, such a scheme probably does not preserve the maximum principle (to this respect, note in particular that taking large values of the parameter β makes the reconstructed profile very close to a step, which makes this choice of y_σ very close to the downwind choice). A more reasonable choice (the one performed in this paper) it to evaluate the flux crossing σ by a characteristic method, which is equivalent to use Equation (5) with the following choice for y_σ:

$$y_\sigma = \frac{1}{\nu}\int_{1-\nu}^1 \tilde{y}(x)\ \mathrm{d}x,$$

with ν the CFL number defined by (6). Since the primitive function of $\tilde{y}$ is known, using Equation (18) to compute x_0 yields y_σ.

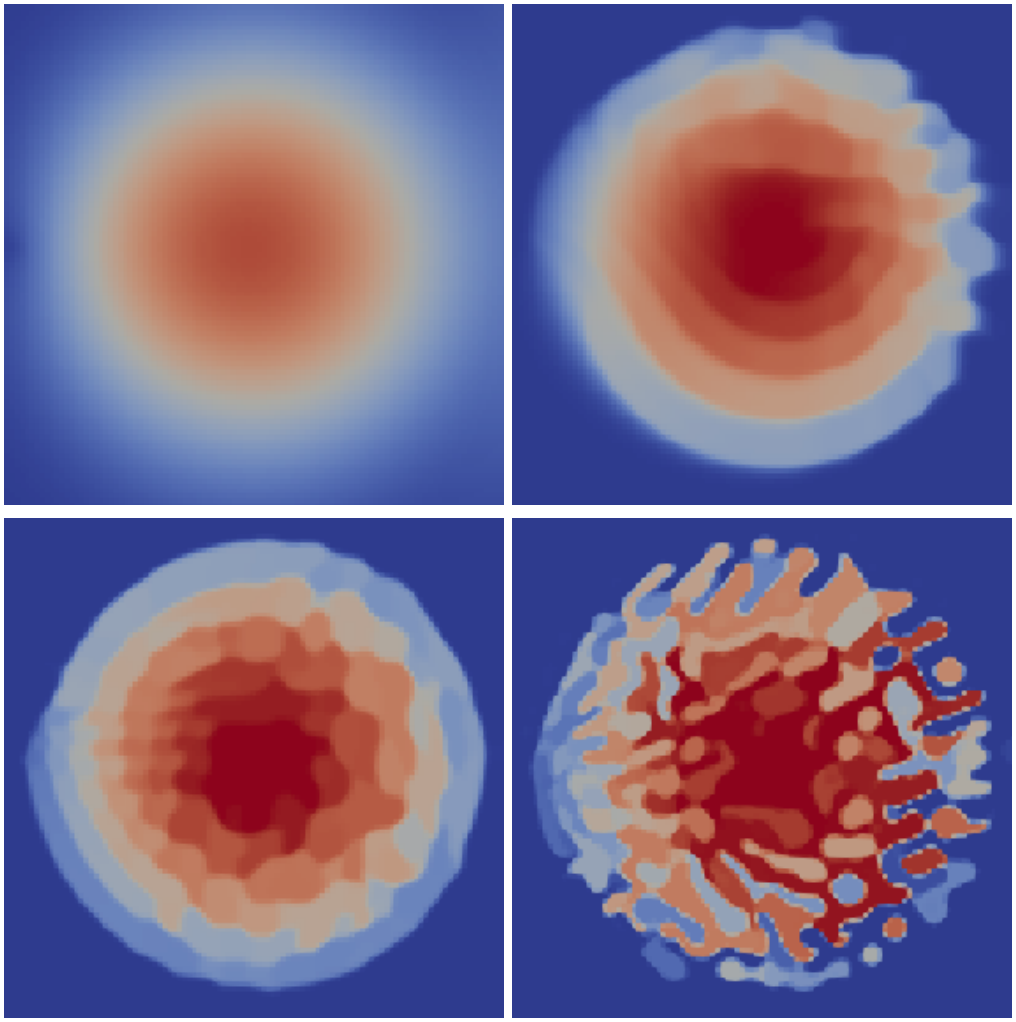

FIGURE 17. Rotation of the characteristic function of a circle – Results obtained at $t = 2\,\pi$ with the alternate-directions algorithm based on the upwind scheme (top left), the MUSCL scheme (top right), the THINC scheme (bottom left) and the anti-diffusive scheme (bottom right). The blue and red colors correspond to $y = 0$ and $y = 1$, repectively. Only the middle-left part of the computational domain is shown.

APPENDIX B. TRANSPORT OF A REGULAR FUNCTION

We consider in this section the same convection field as in Section 4.2, namely a uniform rotation of unity angular velocity, with a regular initial condition:

$$y = \left| \begin{array}{ll} 0.25 - r^2 & \text{if } r \leq 0.5 \\ 0 & \text{otherwise} \end{array} \right. , \text{ with } r = \left[(x_1 - 0.5)^2 + (x_2 - 0.5)^2 \right]^{1/2}.$$

Results at $t = 2\,\pi$ (so after half a rotation) are given on Figure 17. As expected, the compressive behaviour of the anti-diffusive scheme dramatically affects the aspect of the solution. The same phenomenon is observed, but with a very lower impact, for the THINC scheme. Note that all the schemes tested in this study are however consistent (in fact, convergent), so the correct solution is progressively retrieved when refining the space discretization and reducing accordingly the time step (results not shown here).

References

[1] O. Bokanowski and H. Zidani. Anti-dissipative schemes for advection and application to Hamilton-Bellmann equations. *Journal of Scientific Computing*, 30:1–33, 2007.

[2] T. Bonometti and J. Magnaudet. An interface-capturing method for incompressible two-phase flows. validation and application to bubble dynamics. *International Journal of Multiphase Flow*, 33:109–133, 2007.

[3] CALIF^{3}S. A software components library for the computation of fluid flows. `https://gforge.irsn.fr/gf/project/califs`.

[4] D.A. Cassidy, J.R. Edwards, and M. Tian. An investigation of interface-sharpening schemes for multi-phase mixture flows. *Journal of Computational Physics*, 228:5628–5649, 2009.

[5] B. Després and F. Lagoutière. Contact discontinuity capturing scheme for linear advection and compressible gas dynamics. *Journal of Scientific Computing*, 16:479–524, 2002.

[6] T. Gallouët, R. Herbin, and Latché. On the weak consistency of finite volumes schemes for conservation laws on general meshes. *SeMA Journal*, 76:581–594, 2019.

[7] E. Godlewski and P.-A. Raviart. Numerical approximation of hyperbolic systems of conservation laws. Number 118 in Applied Mathematical Sciences. Springer, New York, 1996.

[8] F.H. Harlow and A.A. Amsden. A numerical fluid dynamics calculation method for all flow speeds. *Journal of Computational Physics*, 8:197–213, 1971.

[9] F.H. Harlow and J.E. Welsh. Numerical calculation of time-dependent viscous incompressible flow of fluid with free surface. *Physics of Fluids*, 8:2182–2189, 1965.

[10] A. Harten. High resolution schemes for hyperbolic conservation laws. *Journal of Computational Physics*, 49:357–393, 1983.

[11] F. Kemm. A comparative study of TVD limiters – well-known limiters and an introduction of new ones. *International Journal for Numerical Methods in Fluids*, 67:404–440, 2011.

[12] P.D. Lax and B. Wendroff. Systems of conservation laws. *Communications in Pure and Applied Mathematics*, 13:217–237, 1960.

[13] L. Piar, F. Babik, R. Herbin, and J.-C. Latché. A second order cell centered scheme for convection-diffusion equations on unstrutured non-conforming grids. *International Journal for Numerical Methods in Fluids*, 71:873–890, 2013.

[14] A.J. Rider and D.B. Kothe. Reconstructing volume tracking. *Journal of Computational Physics*, 141:112–152, 1998.

[15] E. Toro. *Riemann solvers and numerical methods for fluid dynamics – A practical introduction (third edition)*. Springer, 2009.